

AFFDL-TR-75-51

ADA 021 286

FRACTURE MECHANICS ANALYSIS OF AN ATTACHMENT LUG

*AEROELASTIC AND STRUCTURES RESEARCH LABORATORY
DEPARTMENT OF AERONAUTICS AND ASTRONAUTICS
MASSACHUSETTS INSTITUTE OF TECHNOLOGY
CAMBRIDGE, MASSACHUSETTS 02139*

JANUARY 1976

TECHNICAL REPORT AFFDL-TR-75-51

Approved for public release; distribution unlimited

AIR FORCE FLIGHT DYNAMICS LABORATORY
Air Force Systems Command
Wright-Patterson Air Force Base, Ohio 45433

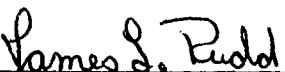
2006092/098

NOTICE


When Government drawings, specifications, or other data are used for any purpose other than in connection with a definitiely related Government procurement operation, the United States Government thereby incurs no responsibility nor any obligation whatsoever; and the fact that the Government may have formulated, furnished, or in any way supplied the said drawings, specifications, or other data, is not to be regarded by implication or otherwise as in any manner licensing the holder or any other person or corporation, or conveying any rights or permission to manufacture, use, or sell any patented invention that may in any way be related thereto.


This report has been reviewed by the Information Office (OI) and is releasable to the National Technical Information Service (NTIS). At NTIS, it will be available to the general public, including foreign nations.

"This technical report has been reviewed and is approved for publication."


JAMES L. RUDD
Project Engineer

FOR THE COMMANDER


ROBERT M. BADER, Chief
Structural Integrity Branch
Structures Division


Gerald G. Leigh, Lt Col, USAF
Chief, Structures Division

Copies of this report should not be returned unless return is required by security considerations, contractual obligations, or notice on a specific document.

UNCLASSIFIED

SECURITY CLASSIFICATION OF THIS PAGE (When Data Entered)

REPORT DOCUMENTATION PAGE		READ INSTRUCTIONS BEFORE COMPLETING FORM
1. REPORT NUMBER AFFDL-TR-75-51	2. GOVT ACCESSION NO. N/A	3. RECIPIENT'S CATALOG NUMBER N/A
4. TITLE (and Subtitle) FRACTURE MECHANICS ANALYSIS OF AN ATTACHMENT LUG		5. TYPE OF REPORT & PERIOD COVERED INTERIM May 1974-October 1974
		6. PERFORMING ORG. REPORT NUMBER ASRL TR 177-1
7. AUTHOR(s) Oscar Orringer		8. CONTRACT OR GRANT NUMBER(s) F33615-74-C-3063
9. PERFORMING ORGANIZATION NAME AND ADDRESS Aeroelastic and Structures Research Lab. Department of Aeronautics & Astronautics MIT, Cambridge, Massachusetts 02139		10. PROGRAM ELEMENT, PROJECT, TASK AREA & WORK UNIT NUMBERS 13670315
11. CONTROLLING OFFICE NAME AND ADDRESS Air Force Flight Dynamics Laboratory Air Force Systems Command Wright-Patterson AFB, Ohio 45433		12. REPORT DATE January 1976
14. MONITORING AGENCY NAME & ADDRESS (If different from Controlling Office) Same		13. NUMBER OF PAGES 83
		15. SECURITY CLASS. (of this report) Unclassified
		15a. DECLASSIFICATION/DOWNGRADING SCHEDULE N/A
16. DISTRIBUTION STATEMENT (of this Report) Approved for public release; distribution unlimited.		
17. DISTRIBUTION STATEMENT (of the abstract entered in Block 20, if different from Report) Same		
18. SUPPLEMENTARY NOTES None		
19. KEY WORDS (Continue on reverse side if necessary and identify by block number) Fracture Mechanics Hybrid Elements Stress Intensity Factors Aircraft Structural Integrity Finite Element Analysis Stress Analysis Computer Structural Analysis		
20. ABSTRACT (Continue on reverse side if necessary and identify by block number) This report documents a finite-element analysis procedure for computation of Mode I and Mode II stress intensity factors associated with a sharp crack in an attachment lug detail. The procedure is a complete FORTRAN-IV program which generates and parametrically analyzes the lug, based on designer-oriented input data. The formulation of a special crack-containing element is reviewed and its performance is summarized. A detailed description of the		

UNCLASSIFIED

SECURITY CLASSIFICATION OF THIS PAGE(When Data Entered)

lug analysis procedure covers the physical problem, modeling, program flow and options, input/output conventions, execution times and limitations which must be observed. Results from example analyses of some attachment lugs are presented.

UNCLASSIFIED

SECURITY CLASSIFICATION OF THIS PAGE(When Data Entered)

FOREWORD

The developments documented in this report were carried out at the Aeroelastic and Structures Research Laboratory (ASRL), Department of Aeronautics and Astronautics, Massachusetts Institute of Technology, Cambridge, Massachusetts 02139, under Contract No. F33615-74-C-3063 (Project 1367, Task 136703) from the U.S. Air Force Flight Dynamics Laboratory. Mr. James L. Rudd (AFFDL/FBE) served as technical monitor. The contractor's report number is ASRL TR 177-1.

TABLE OF CONTENTS

<u>Section</u>	<u>Page</u>
1. INTRODUCTION	1
2. BASIC ELEMENTS AND METHODS	3
2.1 Element QUAD4	3
2.2 Element PCRK59	5
3. ATTACHMENT LUG PROGRAM	13
3.1 Lug Structure Model	13
3.2 Input Conventions	14
3.3 Required Subprograms and Other Features	17
3.4 Model Generation and Program Flow	18
3.5 Output Conventions and Error Messages	20
3.6 Visual Interpretation of Output	21
3.7 Program Status	22
4. RESULTS OF EXAMPLE ANALYSES	23
4.1 Analysis of Wing Root Attachment Lug	23
4.2 Analysis of Engine Pylon Truss Lug	24
4.3 Example Application	28
5. CONCLUSIONS	30
REFERENCES	32
FIGURES	34
APPENDIX A	67

LIST OF FIGURES

<u>Figure</u>		<u>Page</u>
1	Combination of Assumed-Displacement Elements with Hybrid Crack-Containing Element	34
2	Conventions for ASRL QUAD4 Assumed-Displacement Element	34
3	ASRL PCRK59 Hybrid Crack-Containing Element	35
4	Application of PCRK59 Element to Symmetric Analyses	36
5	Attachment Lug Detail	37
6	Crack Parameters	37
7	Program LUG Input Conventions	38
8	Finite Element Mesh for NT=3	39
9	Hypothetical Wing Root Attachment Lug	40
10	Input Data for Analysis of Lug shown in Figure 9	41
11	Program LUG Flow Chart	42
12	Printout of Input Data	45
13	Numbering Conventions Illustrated for Sample Mesh shown in Figure 8	46
14	Overlay for Stress Intensity Analysis	48
15	Force and Displacement Tables from Stress Analysis . .	49
16	Part of Stress Table	50
17	Stress Intensity Factor Table from Analysis with NT=4	51
18	Stress Contours for Wing Root Lug	52
19	Butterfly Plot for Wing Root Lug Stress Intensities .	54
20	Interpretation of Butterfly Plots	55
21	Scale Mesh Plan for Engine Pylon Truss Lug	56

LIST OF FIGURES (continued)

<u>Figure</u>		<u>Page</u>
22	Stress Contours for Engine Pylon Truss Lug (Tension Bearing, Cosine Pressure)	57
23	Butterfly Plot for Engine Pylon Truss Lug (Tension Bearing, Cosine Pressure)	58
24	Scale Mesh Plan for 7-Inch Engine Pylon Truss Lug . .	59
25	Effect of Shank Length on Stress Intensity (Tension Bearing, Cosine Pressure)	60
26	Comparison of Cosine and Uniform Pressure Distributions (Tension Bearing)	61
27	Stress Contours for 7-Inch Engine Pylon Truss Lug (Tension Bearing, Uniform Pressure)	62
28	Stress Contours for 7-Inch Engine Pylon Truss Lug (Positive Shear Bearing, Cosine Pressure)	63
29	Comparison of Finite Element Results with Engineering Beam Theory (Positive Shear Bearing, Cosine Pressure). .	64
30	Butterfly Plots for 7-Inch Engine Pylon Truss Lug (Positive Shear Bearing, Cosine Pressure)	65
31	Butterfly Plots for 7-Inch Engine Pylon Truss Lug (Positive Shear Bearing, Uniform Pressure)	65
32	Butterfly Plots for 7-Inch Engine Pylon Truss Lug (Compression Bearing, Cosine Pressure)	66
33	Butterfly Plots for 7-Inch Engine Pylon Truss Lug (Compression Bearing, Uniform Pressure)	66

Section 1

INTRODUCTION

The application of linear elastic fracture mechanics analysis to structural details in new aircraft designs has received growing emphasis from the Air Force and from aircraft manufacturers during the past few years. Not only have fracture mechanics data become more readily available in recent years [1,2], but also, there has been a trend toward treatment of the problem of fracture in its own right, distinct from fatigue. Within the past year, this trend has culminated in the establishment of structural design criteria by the Air Force which require an aircraft designer to take specific design-analysis actions to protect structures against fracture [3]. Required design calculations now include, generally, comparison of load-induced stress intensity factors to material fracture toughness and assessment of crack growth rates, based on assumptions concerning the size and location of possible cracks in the structure. Both types of calculation require prior estimation of the load-induced stress intensity factor. Hence, there has also been considerable emphasis on adding to the body of available fracture mechanics solutions.

Because so few geometrical configurations are amenable to a purely analytical solution of the equations of elastic fracture mechanics, the finding of new solutions depends upon development of numerical analysis techniques. Extensive contributions have been made by Bowie and his colleagues [4,5,6] using the complex variable formulation of elasticity in combination with conformal mapping, analytic continuation and boundary collocation methods. Tada, et al. [7] have recently collected and classified a comprehensive body of solutions based on the semi-analytical methods (complex variables, boundary collocation, Fourier transforms, etc.) among which appear many new solutions by Tada. However, the semi-analytical methods have not as yet proved capable of application to the irregular geometrical configurations which are found so often

in real airframe structural details. Stress analysis of irregular structure has been the province of the finite-element methods for the past decade. Within the last six years, numerous contributors have extended the finite-element technique to fracture mechanics analysis.

Work on finite-element fracture mechanics analysis at MIT has followed the path of assumed-stress hybrid elements, first proposed by Pian [8] for ordinary continuum elements. The hybrid method was subsequently extended by Tong, Pian, Luk, and Lasry [9,10,11,12] to formulation of rectangular elements which incorporate an elastic crack-tip singularity, but which also have an assumed linear or quadratic variation of displacements along the element edges and are thus compatible with ordinary elements (Figure 1). Numerical experiments have demonstrated that the hybrid crack-containing elements are capable of producing estimates of K_I and K_{II} with less than 1 percent error, using 20 to 50 total degrees of freedom in the analysis, for simple geometrical configurations. Hence, it becomes possible to create economically practical analysis procedures for structural details by refining the mesh of ordinary elements to pick up the stress gradients caused by nonuniform loading and complicated boundary geometry, leaving to the special hybrid element the task of picking up the local gradients caused by the crack-tip singularity.

This report summarizes recent developments at the MIT Aeroelastic and Structures Research Laboratory (ASRL) in which the crack-containing hybrid element has been applied for the first time to some typical structural details, found in current production aircraft, with geometries too complicated for economical solution by other techniques. The "PCRK59" crack element used in these analyses is a generalized version of the original Lasry element [12] which was formulated and programmed by Tong and subsequently modified for greater utility by the ASRL computing staff.

Section 2

BASIC ELEMENTS AND METHODS

2.1 Element QUAD4

The ASRL QUAD4 four-node quadrilateral element (Figure 2) is used as the basic building block in the analysis procedure. QUAD4 is the well-known bilinear isoparametric assumed-displacement element which has been used for continuum stress analysis for many years [13]. The ASRL version has been programmed as an independent subroutine which includes the options of individual rotation transformations at each node and calculation of a "B" matrix for stress analysis.

The nodal coordinates $X_1, Y_1, X_2, \dots, Y_4$, element thickness T and the elastic constants matrix:

$$\tilde{C} = \begin{bmatrix} C_{11} & C_{12} & C_{13} \\ C_{12} & C_{22} & C_{23} \\ C_{13} & C_{23} & C_{33} \end{bmatrix} ; \quad \begin{Bmatrix} \sigma_{xx} \\ \sigma_{yy} \\ \sigma_{xy} \end{Bmatrix} = \tilde{C} \begin{Bmatrix} \epsilon_{xx} \\ \epsilon_{yy} \\ \epsilon_{xy} \end{Bmatrix} \quad (1)$$

comprise the required basic input information. For isotropic materials

$$\tilde{C} = \frac{E}{1-\nu^2} \begin{bmatrix} 1 & \nu & 0 \\ \nu & 1 & 0 \\ 0 & 0 & \frac{1-\nu}{2} \end{bmatrix} \quad \text{or} \quad \frac{E}{(1+\nu)(1-2\nu)} \begin{bmatrix} 1-\nu & \nu & 0 \\ \nu & 1-\nu & 0 \\ 0 & 0 & \frac{1-2\nu}{2} \end{bmatrix} \quad (2)$$

(plane stress) (plane strain)

Subroutine QUAD4 allows for general plane orthotropic behavior, a capability which is included in the attachment lug program. Plane stress is assumed in the analysis. The lug program does not use the rotation transformation option.

The element stiffness matrix \tilde{k} is calculated by numerical area integration, using 3x3-point Gaussian quadrature [14] for

$$\underset{\sim}{k} = \frac{1}{\text{AREA}} \iint \underset{\sim}{D}^T \underset{\sim}{C} \underset{\sim}{D} dX dY \quad (3)$$

where $\underset{\sim}{D}$ contains the interior strain-nodal displacement relations:

$$\{\epsilon_{xx} \ \epsilon_{yy} \ \epsilon_{xy}\} = \underset{\sim}{D}(x, y) \{q_1 \ q_2 \ \dots \ q_8\} \quad (4)$$

The stiffnesses are returned in Lower Triangle Vector (LTV) form:

$$\underset{\sim}{k} = [k_{11} \ k_{21} \ k_{22} \ k_{31} \ k_{32} \ \dots \ k_{88}] \quad (5)$$

For the purpose of stress analysis, Eqs. 1 and 4 may be combined to give:

$$\underset{\sim}{\sigma}(x, y) = \underset{\sim}{C} \underset{\sim}{D}(x, y) \underset{\sim}{q} = \underset{\sim}{B}(x, y) \underset{\sim}{q} \quad (6)$$

QUAD4 also returns the matrix $\underset{\sim}{B}(X_c, Y_c)$, formed at the fifth Gaussian station, for later calculation of stresses at the element "centroid", defined in terms of the nodal coordinates:

$$X_c = \frac{1}{4} \sum_{i=1}^4 X_i \quad Y_c = \frac{1}{4} \sum_{i=1}^4 Y_i \quad (7)$$

The behavior of QUAD4 has been studied extensively on other projects and is well understood. Uniform or nearly uniform stress fields can be picked up to within the roundoff accuracy of the digital computer being used for the analysis. The inability of the bilinear assumed displacement fields to follow the quadratic deflection of the neutral axis of a cantilever beam loaded by an end moment has been well documented elsewhere [15] and constitutes a limitation on the QUAD4. In practical terms, this requires that the element aspect ratio (Figure 2) be held close to unity for models of structures which are expected to have quadratic or higher-order displacement behavior. In some cases, even an aspect ratio of unity is not sufficient to insure convergence of the solution. For example, the

QUAD4 element was used recently to model a thick-walled cylinder subjected to centrifugal loading from its own mass, due to rotation [16]. The analytical solution of this axisymmetric problem includes an r^3 term in the radial displacement field which the bilinear element is unable to pick up; errors of 25% were found for a cylinder with a 2:1 ratio of outside-to-inside radius, using four unit-aspect-ratio QUAD4 elements through the wall thickness.

The misbehavior of the bilinear element in the presence of higher-order gradients requires the use of many elements to model complicated geometries. Also, "calibration" of the finite-element model is a good idea, where possible, by comparing the numerical results with independent solutions. Calibrations for this project have included comparisons with the classical elasticity solution for stresses and displacements near a circular hole in a semi-infinite strip under tension [17] and with finite-element analyses using higher-order assumed-displacement elements.

2.2 Element PCRK59

Formulation of the assumed-stress hybrid finite-element method begins with the Principle of Minimum Complementary Energy:

$$\pi_c = \sum_n \left[\int_{S_u} \hat{\underline{u}}^T \underline{T} dS - \int_V \frac{1}{2} \underline{\sigma}^T \underline{S} \underline{\sigma} dV \right] \quad (8)$$

where

\sum_n indicates summation over the element set.

S_u = part of the element boundary over which displacements are prescribed.

V = element volume.

$\hat{\underline{u}}$ = vector of prescribed displacements on S_u .

$\underline{\sigma}$ = stress vector.

\underline{S} = compliance constants = \underline{C}^{-1} ($\underline{\epsilon} = \underline{S}\underline{\sigma}$).

\underline{T} = vector of surface tractions = $\underline{N}\underline{\sigma}$, where \underline{N} is a matrix of surface normal direction cosines.

If Π_c is used directly, only the stress field is assumed, subject to admissibility criteria requiring that the assumed stresses satisfy:

- (i) Interior equilibrium $\partial \sigma_{ij} / \partial x_j + \hat{F}_i = 0$, in V , where \hat{F}_i are prescribed body forces.
- (ii) Mechanical boundary conditions $\tilde{N}\tilde{\sigma} = \hat{T}$ on S_σ , that part of the element boundary over which the surface tractions \hat{T} are prescribed.
- (iii) Equilibrium of surface tractions $\tilde{N}\tilde{\sigma}$ across the interelement boundaries S , which are distinct from S_u and S_σ .

Formal application of the variational calculus to Eq. 8 leads to two sets of Euler equations:

- (iv) Interior compatibility, $\tilde{S}\tilde{\sigma} = \tilde{\epsilon}$ in V , where $\tilde{\epsilon}_{ij} = 1/2 (\partial u_i / \partial x_j + \partial u_j / \partial x_i)$.
- (v) Displacement boundary conditions, $\tilde{u} = \hat{u}$ on S_u .

If assumed stress functions are substituted and Eq. 8 is integrated before Π_c is varied, there results a linear equation system in which the generalized coordinates to be solved for are forces. This approach leads to a Matrix Force Method analysis which brings with it the programming problem of systematic identification and elimination of redundant quantities.

The assumed-stress hybrid approach avoids the complications of force redundancy by modifying Π_c so that the primary unknowns in a finite-element application become displacements once again. The Principle of Minimum Complementary Energy is modified by addition of Lagrange multiplier terms [8,18] which change admissibility criteria. Specifically, conditions (ii) and (iii) above are relaxed and condition (v) is enforced. Under the new principle, stress functions satisfying only the interior equilibrium conditions (i) may be assumed, and displacement functions which satisfy interelement compatibility and conditions (v) must now be assumed as well. The modified energy principle which replaces Eq. 8 is:

$$\pi_1 = \sum_n \left[\int_{\partial V} \tilde{T}^T \tilde{u} dS - \int_V \frac{1}{2} \tilde{\sigma}^T \tilde{S} \tilde{\sigma} dV - \int_{S_\sigma} \tilde{u}^T \hat{T} dS \right] \quad (9)$$

where " ∂V " represents the entire element boundary, $S + S_u + S_\sigma$. To convert π_1 into a finite-element formulation, the stress vector $\tilde{\sigma}$ is assumed within each element and the displacement vector \tilde{u} is assumed on the boundary, ∂V , of each element:

$$\tilde{\sigma} = \tilde{P}(x, y, z) \tilde{\beta} \quad \tilde{u} = \tilde{L}(x, y, z) \tilde{q} \quad (10)$$

where \tilde{P} and \tilde{L} are matrices of interpolation functions. Vector $\tilde{\beta}$ contains generalized stress coordinates, while \tilde{q} is a vector of nodal displacements. Matrices \tilde{P} and \tilde{L} are assumed independently, with \tilde{L} defined only along the element boundary ∂V . Substitution of Eq. 10 into Eq. 9 then leads to:

$$\pi_1 = \sum_n \left[\tilde{\beta}^T \tilde{G} \tilde{q} - \frac{1}{2} \tilde{\beta}^T \tilde{H} \tilde{\beta} - \tilde{q}^T \hat{\tilde{Q}} \right] \quad (11)$$

where

$$\tilde{G} = \int_{\partial V} (\tilde{N} \tilde{P})^T \tilde{L} dS \quad \tilde{H} = \int_V \tilde{P}^T \tilde{S} \tilde{P} dV$$

$$\hat{\tilde{Q}} = \int_{S_\sigma} \tilde{L}^T \hat{T} dS = \text{Consistent nodal force vector} \quad (12)$$

and where $\tilde{N}\tilde{\sigma} = \tilde{N}\tilde{P}\tilde{\beta}$ has been substituted for the surface traction vector \tilde{T} in the expression for \tilde{G} .

Direct assembly and solution of the equation system represented by π_1 is possible, but results in a mixed matrix method, with both force and displacement unknowns. A more versatile formulation is obtained by recognizing that, since the stresses are assumed independently within each element, $\tilde{P}\tilde{\beta}$ for one element is not coupled with any other elements. Therefore, the unknowns $\tilde{\beta}$ may be formally eliminated by applying the variational calculus to π_1 :

$$\delta \pi_1 (\tilde{\beta} \text{ for only one element varied}) = \delta \tilde{\beta}^T \{ \partial \pi_1 / \partial \tilde{\beta} \} =$$

$$\delta \tilde{\beta}^T (\tilde{G} \tilde{q} - \tilde{H} \tilde{\beta}) = 0$$

which leads to

$$\underline{Q} = \underline{H}^{-1} \underline{G} \underline{q} \quad (13)$$

Substitution of Eq. 13 back into Eq. 11 then yields*:

$$\pi_1 = \sum_n \left[\frac{1}{2} \underline{q}^T \underline{G}^T \underline{H}^{-1} \underline{G} \underline{q} - \underline{q}^T \underline{\hat{Q}} \right] \quad (14)$$

The alternate expression for π_1 given by Eq. 14 represents a pure Matrix Displacement Method. The quantity $\underline{G}^T \underline{H}^{-1} \underline{G}$ can be recognized as an element stiffness matrix. The \sum_n notation may now be identified as a conventional Matrix Displacement Method structure model assembly procedure. Hence, structure models can be created by assembling conventional and hybrid elements, provided only that compatibility across the interelement boundaries is maintained by proper choices for the assembed displacement fields. The versatility of the hybrid method lies in its ability to provide special-purpose elements, for restricted regions, which may be coupled into a model containing conventional elements in the remaining regions which are free of singularities or other unusual behavior.

The original hybrid crack elements [9,10] were derived from π_1 by assuming a stress field containing $r^{-1/2}$ terms, where r measures radial distance from the crack tip and, by assuming displacement fields which vary linearly from one node to the next, along the element boundary. However, subsequent analysis of error sources [19] has indicated that the area integration required for computation of \underline{H} (see Eqs. 12) gives poor results for the $r^{-1/2}$ terms since some of the Gaussian stations are close to the crack tip. This situation may be remedied by increasing the number of Gaussian stations, but the computation of \underline{k} then becomes too costly. A better approach, used for the second-generation crack elements [11,12] has been followed in the present work. The energy principle π_1 may be further modified by introducing two displacement fields: \bar{u} assumed on ∂V and u assumed in V . There now arises another compatibility condition, $u = \bar{u}$ on ∂V , which is relaxed by the Lagrange

*Note that \underline{H} and \underline{H}^{-1} are symmetric matrices.

multiplier method. At the same time, the condition that \underline{u} must satisfy the interior equilibrium equations, as well as the strain-displacement relations, is enforced. As a result, the area integration is converted to a boundary integral and Π_1 is modified to the form:

$$\Pi_2 = \sum_n \left[\int_{\partial V} \underline{T}^T \underline{\bar{u}} dS - \frac{1}{2} \int_{\partial V} \frac{1}{2} (\underline{T}^T \underline{u} + \underline{u}^T \underline{T}) dS - \int_{S_r} \underline{\bar{u}}^T \hat{\underline{T}} dS \right] \quad (15)$$

The same boundary displacement field $\underline{\bar{u}}$ can be used for both Π_1 and Π_2 . However, the interior assumed fields in Π_2 must be a complete elasticity solution: stresses $\underline{\sigma}$ and displacements \underline{u} which satisfy all of the equations of elasticity, with $\underline{T} = \underline{N}\underline{\sigma}$ a derived quantity. The distributions for $\underline{\sigma}$ and \underline{u} are obtained from a complex variable solution of the equations of elasticity near a crack tip or equivalently, by solving the biharmonic equation for an Airy stress function. Computation of the element stiffness matrix is the same as for Π_1 , except that \underline{H} is now computed by a boundary integral:

$$\underline{H} = \frac{1}{2} \int_{\partial V} [(\underline{N}\underline{P})^T \underline{A} + \underline{A}^T \underline{N}\underline{P}] dS \quad (16)$$

where \underline{A} is a matrix of shape functions corresponding to the interior assumed displacement field, $\underline{u} = \underline{A}\underline{q}$.

The principle Π_2 also possesses the advantage of convenience for treatment of arbitrary shapes, since only boundary integration is required. Figure 3 illustrates the PCRK59 element based on Π_2 . Input information required by this element is similar to the information required by QUAD4:

- (i) Geometry: global coordinates of the crack tip X_t, Y_t ; global coordinates of each node $X_1, Y_1, X_2, \dots, Y_9$.
- (ii) Material properties: the shear modulus $G = E/2(1+\nu)$ and a second constant $\eta = (3-\nu)/(1+\nu)$ for plane stress (3-4 ν for plane strain)

PCRK59 is programmed only for isotropic material and does not incorporate the rotation transformations available in QUAD4. In fact, rotation transformations cannot be applied once the PCRK59

stiffness matrix has been formed. This limitation is caused by the appearance of the crack tip coordinates in the numerical integration scheme, but the restriction does not affect many practical fracture mechanics problems. The numerical integration is by five-point Gaussian quadrature [14] between each pair of nodes, except that the crack surfaces are skipped. Omission of the crack surfaces is justified because they constitute S_0 , over which $\hat{T} = 0$, and because the derived tractions \tilde{T} satisfy this stress-free condition at least in an average sense.

The PCRK59 element has two other important features. First, unit thickness is assumed. Second, a symmetric "half-element" option is available, under which nodes 1,5 and the crack tip are assumed to lie on a line parallel to the global X-axis, while the element and applied loading are assumed to be symmetric about this line. Under these conditions, a half-model of a structure may be analyzed to obtain Mode I stress intensity solutions only; e.g., for the coupon in uniform tension with edge cracks, shown in Figure 4. The "half-element" consists of nodes 1,2,...5, only, with node 1 requiring a roller restraint to maintain the assumed symmetry. Another input parameter determines which option is executed:

KEY = 1 for "half-element"

2 for full element

The "half-element" option is used mainly for illustrative examples and performance testing. The full element option has been used exclusively in the present work.

Element PCRK59 computes and returns a stiffness matrix in LTV form (see Eq. 5) for either the 10 degree-of-freedom "half-element" or the 18 degree-of-freedom full element. In addition, a special \tilde{B} matrix for calculation of stress intensities is returned. Eq. 13, used in the derivation of the stiffness matrix, can also be used to compute the generalized stress coordinates $\tilde{\beta}$ after the element nodal displacements \tilde{q} have been obtained. For the PCRK59,

$$\tilde{\beta} = \{k_1 \beta_2 \beta_3 \cdots \beta_9 k_2 \beta_{11} \cdots \beta_{18}\} \quad (17)$$

where k_1, k_2 , are the Mode I, Mode II stress intensity factors, defined by:

$$\begin{aligned}\sigma_{xx} &= \frac{k_1}{\sqrt{2r}} f_1(\theta) + \frac{k_2}{\sqrt{2r}} f_2(\theta) + (\text{terms in } \beta_2, \beta_3 \dots) \\ \sigma_{yy} &= \text{etc.} \dots\end{aligned}\quad (18)$$

The functions f_1, f_2 , are from the classical crack tip solution, and the other generalized coordinates $\beta_2, \beta_3, \dots, \beta_{18}$ represent far-field behavior. Thus, \tilde{B} is formed by extracting the first and tenth rows of $\tilde{H}^{-1}\tilde{G}$, so that the stress intensities may be calculated from:

$$\{k_1 \ k_2\} = \tilde{B}_{(2 \times 18)} \{g_1 \ g_2 \ \dots \ g_{18}\} \quad (19)$$

for the full element. Only the first row of $\tilde{H}^{-1}\tilde{G}$ is extracted if the "half-element" option is in effect:

$$k_1 = \tilde{B}_{(1 \times 10)} \{g_1 \ g_2 \ \dots \ g_{10}\} \quad (20)$$

NASA/ASTM standard stress intensity factors may be computed after Eq. 19 or Eq. 20 by:

$$K_I = k_1 \sqrt{\pi} \quad K_{II} = k_2 \sqrt{\pi} \quad (21)$$

If a structure model with thickness $T \neq 1$ is to be analyzed, this may be done simply by scaling the PCRK59 stiffness to:

$$\tilde{k}' = T \tilde{k} \quad (22)$$

Performance of the PCRK59 element has been tested extensively by comparison with classical and boundary collocation solutions [19]. Solutions for K_I accurate to better than 1 percent have been obtained with a rectangular crack element surrounded by only a few QUAD4 elements. Other tests have shown that solution accuracy within 3 percent is maintained when the crack element shape is distorted by relocating some nodes as much as $0.3 \times$ (length of crack within element) away from the positions they occupy for a rectangle. Also, the 3 percent accuracy limit can be maintained with the crack tip located anywhere from 20 to 70 percent across a line between

nodes 5 and 1, with the element shape kept rectangular. The distortions of element shape and crack tip location required for the structure models analyzed in the present work are well within these limits.

The PCRK59 element possesses one unavoidable quirk which arises from its linearity. If the element is placed in a region with compressive stress normal to the crack, a negative value of K_I is obtained. In a real structure, the crack would close and cease to be a problem in this situation. Therefore, negative K_I values should be interpreted as signaling the absence of Mode I stress intensity. On the other hand, the solution for K_{II} will be positive (negative) according to whether the crack is being subjected to positive (negative) shear stress, as defined by the standard conventions of elasticity. In this case, the correct interpretation is to take the absolute value of K_{II} .

In summary, the PCRK59 element permits efficient computation of stress intensity factors by well established procedures of the Matrix Displacement Method. The unusual features of the element are internal to its subroutine. The element subroutine requires familiar input information and returns k and B matrices like a conventional element. The structure model is assembled and a global displacement solution is computed by standard techniques. Computation of either the centroid stresses in the conventional elements or the stress intensity factors in the crack element is then merely a matter of extracting the element displacements q from the global solution and performing a straightforward matrix multiplication.

Section 3

ATTACHMENT LUG PROGRAM

Program LUG has been developed for analysis of stresses or stress intensity factors in an attachment lug typical of many structural details found in current aircraft. This section describes the lug structure model and explains how the program is used. Results obtained from some example analyses are presented in Section 4.

3.1 Lug Structure Model

Figure 5 illustrates the structure which Program LUG models. The detail consists of a straight shank, built in at the foot and a rounded ear whose outer edge is concentric with a bearing pinhole. Provision is made to treat the lug as a two-material system composed of an isotropic bushing ring surrounding the bearing pinhole, and the lug proper, which may be treated as either isotropic or plane orthotropic. A perfect mechanical bond between the bushing and lug is assumed. A monolithic single-material lug is obtained if identical isotropic material properties are specified for the bushing and the lug proper.

Bearing loads are assumed to be applied to the structure at the bearing pinhole surface. Tension, compression, positive shear or negative shear may be applied. These loads are defined in Figure 5. Each load component is represented as a radial bearing pressure over one-half the circumference of the bearing pinhole, with the pressure distribution centered on and symmetric about the line of action of the load. Options for a cosine pressure distribution or a uniform pressure distribution are available.

The attachment lug is assumed to be under plane stress, with two analysis options allowed. Under option 1, a model of an uncracked lug is assembled, using only QUAD4 elements, and a conventional stress analysis is executed. Under option 2, a small radial crack is assumed to emanate from the bearing pinhole surface,

with the crack tip located in the bushing. The length of the crack is specified by the program user (Figure 6). Program LUG automatically executes a sequence of solutions in which the crack location is varied step-wise around the entire bearing hole circumference.

3.2 Input Conventions

The input data conventions for Program LUG are summarized in Figure 7. Formats for all numerical data have been standardized to I5 fields for integers and E10.0 fields for floating point numbers. Integer data and floating point data supplied in E format should be right-justified in the field. However, floating point data may also be given in F format, if desired, without changing the program code. F format data need not be right-justified. Also, the implied decimal point location for floating point data may be overridden. A maximum of 3 decimal figures may be input under E format and up to 7 decimal figures may be input under F format.

A series of independent cases may be analyzed in one run. The first input data card specifies the total number of cases which follow. The remainder of the input deck consists of six cards per case which give the program a complete description of the case. The conventions for these cards are as follows:

Card 2 - may contain any alphanumeric information which identifies the case. This information is printed as a heading title.

Card 3 - specifies the options selected by the user for four control parameters:

IANL = 1 (Conventional stress analysis without crack).

2 (Stress intensity analysis).

LOAD = 1 (Cosine pressure distribution).

2 (Uniform pressure distribution).

MODE = 1 (Lug treated as isotropic).

2 (Lug treated as orthotropic).

NT = Total number of QUAD4 elements wanted per 45° arc around the bearing pinhole.
A minimum value of 3 is recommended.

Card 4 - specifies the lug dimensions and crack size.

DI = Inside diameter of bearing pinhole.
DB = Outside diameter of bushing.
W = Lug width.
H = Total (root to tip) length of lug.
T = Lug thickness (lug and bushing assumed to have equal thickness).
CSIZE = Length of crack.

Card 5 - specifies the material properties of the bushing, which is always assumed to be isotropic:

E = Young's modulus.
 ν = Poisson's ratio.

Card 6 - specifies the lug material properties. If MODE = 1 on card 3, the convention is:

E = Young's modulus.
 ν = Poisson's ratio.

If MODE = 2 on card 3, the convention is:

E_L = Longitudinal modulus.
 E_{LT} = Cross-coupling modulus.
 E_T = Transverse modulus.
 G_{LT} = Shear modulus.
 θ = Angle between lug XY axes and material LT axes (degree measure, positive CCW from X to L).

Card 7 - specifies the bearing force value:

TENSN = Tension or compression bearing force.
SHEAR = Positive or negative shear bearing force.

The lug dimensions and crack size were defined in Figures 5 and 6. Any value of thickness may be specified. Program LUG rescales the model internally to unit thickness. Figure 8 illustrates a finite element mesh which might result when NT = 3 elements per 45° arc is specified on card 3. The positive convention

for the relationship between the lug XY axes and material LT axes is also shown. The quantities E_L , E_{LT} , E_T , G_{LT} are the conventional plane-orthotropic moduli for; e.g., a fiber composite laminate. The stress-strain relations take the form:

$$\begin{Bmatrix} \sigma_L \\ \sigma_T \\ \sigma_{LT} \end{Bmatrix} = \begin{bmatrix} E_L & E_{LT} & 0 \\ E_{LT} & E_T & 0 \\ 0 & 0 & G_{LT} \end{bmatrix} \begin{Bmatrix} \epsilon_L \\ \epsilon_T \\ \epsilon_{LT} \end{Bmatrix} \quad (23)$$

in the LT axis system. For $\theta \neq 0^\circ$ the stress-strain relations in the XY axis system take a more complicated form:

$$\begin{Bmatrix} \sigma_{XX} \\ \sigma_{YY} \\ \sigma_{XY} \end{Bmatrix} = \begin{bmatrix} C_{11} & C_{12} & C_{13} \\ C_{12} & C_{22} & C_{23} \\ C_{13} & C_{23} & C_{33} \end{bmatrix} \begin{Bmatrix} \epsilon_{XX} \\ \epsilon_{YY} \\ \epsilon_{XY} \end{Bmatrix} = \underset{\sim}{C} \underset{\sim}{\epsilon} \quad (24)$$

where, in general, C_{13} , $C_{23} \neq 0$. The matrix $\underset{\sim}{C}$ in Eq. 24 is computed from E_L , E_{LT} , ..., θ by ASRL subroutine CTFORM.

The bearing load conventions were indicated in Figure 5. The value of TENSXN or SHEAR supplied on card 7 refers to total bearing force; the corresponding pressure distributions are computed internally. A positive (negative) value TENSXN has the effect of applying a tension (compression) bearing load to the structure. A positive (negative) value for SHEAR similarly applies a positive (negative) shear bearing load.

Figure 9 illustrates a portion of the actual finite element mesh generated for a hypothetical large all-aluminum wing root attachment lug. Since the "bushing" diameter does not have any physical significance in this single-material case, it is used to control the mesh so that the tip of a 0.5-inch long crack lies at the middle of the PCRK59 element. The crack is shown with a finite opening for clarity. However, nodes 5 and 6 of the crack element (Figure 3) actually overlap to provide the correct model of a sharp crack. The PCRK59 element has replaced a group of four adjacent

QUAD4 elements in the mesh. When analysis option 2 is in effect, a series of structure models are generated and analyzed one after the other, with the PCRK59 shifted circumferentially by one pair of QUAD4's after each analysis. Thus, for the case shown in Figure 9 (NT = 3), 24 stress intensity solutions are obtained with the crack located successively at $\theta = 0^\circ, 15^\circ, 30^\circ, \dots, 345^\circ$. Figure 10 summarizes the input data deck required to run a stress analysis (case 1) and a stress intensity analysis (case 2) for the hypothetical lug detail.

3.3 Required Subprograms and Other Features

Program LUG requires the following FORTRAN-IV subroutines to form an executable load module:

- (i) ASRL FEABL-2 subroutines ASMLTV, BCON, FACT, ORK, SETUP, SIMULQ, and XTRACT [20,21].
- (ii) ASRL element and utility library subroutines QUAD4, PCRK59, and CTFORM.
- (iii) IBM Scientific Subroutine Package routines MFSD and SINV which are required by the PCRK59 element subroutine.

The entire source deck is supplied in IBM 029-punch format.

The following features of Program LUG may cause machine-dependence problems on non-IBM hardware:

- (i) The 20A4 format for input of case title information may be incompatible with some systems. This may be remedied by changing FORMAT statement 502 to 80A1 and redimensioning vector TITLE to 80.
- (ii) FORTRAN unit numbers 5 and 6 are assumed for the card reader and line printer respectively. Program LUG may be converted to other hardware standards simply by reprogramming the two lines of code:

KR = 5

KW = 6

which appear shortly after the FORMAT statements near the beginning of the program.

- (iii) Program LUG requires a sequential-access scratch dataset, designated as FORTRAN file 20, when analysis option 1 (uncracked structure stresses) is in effect. The file must consist of (30 single-precision words per record) x (records = maximum number of QUAD4 elements expected). A total of 600 records should be adequate for most analyses. A job control instruction, specific to the installation where the program is being executed, is required to create this file on a system disk. However, Program LUG may be executed without creating this file if only stress intensity solutions are sought.
- (iv) IBM/SSP subroutines MFSD and SINV may not be compatible with other systems. If this problem arises, reprogramming or substitution will be required.

3.4 Model Generation and Program Flow

Program LUG automatically generates the geometrical information, element interconnections, etc., which are required to compute and assemble the element stiffnesses, restrain the structure properly, apply the bearing load and execute a stress or stress intensity analysis. The program flow is summarized in Figure 11. Parenthesized numbers in the figure refer to FORTRAN statement numbers in the program listing (Appendix A).

After the input data has been read for a case and some auxiliary values have been calculated, the case title and input data are printed for checking. A sample output from this section of the program is shown in Figure 12. The number of QUAD4 elements required radially in the bushing and lug and the number required axially in the lug shank are then computed by rounding off to the nearest whole number which gives an average element aspect ratio closest to unity for each region. The total number of elements, total degrees of freedom and some additional parameters are then calculated, and the vectors which will contain the K-solutions are erased.

The major section of the code, a loop over the crack locations, then follows. The location loop is executed $8 \times NT$ times for a stress intensity analysis, but only once for a conventional uncracked structure stress analysis. Previous results are erased and the interconnections for an uncracked structure are generated. Figure 13

illustrates the node and element numbering conventions, using the example mesh from Figure 8. The numbering patterns are as follows:

- (i) Nodes are numbered, globally, radially outward from the bearing pinhole on each ray. The rays are taken in counterclockwise order, beginning at $\theta = 0^\circ$. Vertical lines of nodes in the lug shank are numbered afterward, from the top down and from right to left. The last line of nodes is restrained.
- (ii) Degrees of freedom are numbered $2n-1$ (displacement parallel to X) and $2n$ (displacement parallel to Y) at each node n .
- (iii) Elements in the bushing are numbered radially outward and counterclockwise, partially following the node numbering pattern.
- (iv) Elements in the lug ear are numbered radially outward and counterclockwise after the bushing elements.
- (v) Elements in the lug shank are numbered last, from the top down and from right to left.

If a stress intensity analysis is being executed, the location of the PCRK59 element is now computed from the crack location loop index and connections for this element are generated. As shown in Figure 14, the PCRK59 element overlays four QUAD4 elements. The central node of this group of elements is transferred to the bearing pinhole to accommodate the PCRK59. The element numbers of the four overlaid QUAD4 elements are also flagged.

The global XY coordinates for each node in the model are now computed, assuming an uncracked structure. If a stress intensity analysis is being executed, the transferred node coordinates are adjusted and global coordinates are computed for the crack tip. The area corresponding to the global force vector \hat{Q}_G in the FEABL-2 storage system is used as temporary storage for the node coordinate data.

After auxiliary storage for element-level data has been prepared, a loop over all QUAD4 elements is executed. The node coordinates for each element are extracted from the global data, other required input is provided from auxiliary storage and k and B are

computed for the element. Also, centroid coordinates X_c , Y_c are computed for the element; B , X_c , Y_c are stored in FORTRAN file 20 (stress analysis option only) and k is assembled into the global stiffness matrix. If a stress intensity analysis is being executed, these procedures are skipped for the four flagged elements, while k and B are computed and k is assembled for the PCRK59.

After assembly, Q_G is erased and replaced by prescribed nodal forces which are statically equivalent to the specified bearing load and the assumed (cosine or uniform) pressure distribution. For stress intensity analysis, the two nodes at the crack opening each receive one-half the nodal force which would have been applied to a single node at that location in an uncracked structure.

The final section of the code executes a solution of the global equation system and either a stress or a stress intensity analysis. In the latter case, the stress intensity factors are saved and a complete table is printed after the crack location loop has been completed.

3.5 Output Conventions and Error Messages

If a stress analysis has been executed, nodal forces, nodal displacements and element stresses are printed. The table of forces and displacements appears immediately below the problem input data and merely lists the force or displacement value for each degree of freedom ("ROW" in the table heading). The stress table contains one line of information for each element:

Element No., X_c , Y_c , σ_{xx} , σ_{yy} , σ_{xy} , σ_{rr} , $\sigma_{\theta\theta}$, $\sigma_{r\theta}$

The stress values are computed for the element's centroid location X_c , Y_c . Figures 15 and 16 present samples of these output tables.

If a stress intensity analysis has been executed, only a table of K-solutions is printed. Each line of the table corresponds to one crack location, containing:

Angle to crack opening, K_I , K_{II}

A sample is shown in Figure 17.

If abnormal conditions occur during execution, certain error messages may be printed by Program LUG. The messages and actions required are as follows:

- (i) Insufficient core memory available for storage of the problem data causes the message:

THE LENGTH OF THE "DATA" VECTOR FOR THIS CASE IS xxxxx WHICH EXCEEDS yyyyy = THE MAXIMUM ALLOWED IN THE DIMENSION STATEMENT.

The entire run will be terminated if this condition occurs. The dimensions of vectors RE and IN (line 2 of the program code) are yyyyy. Redimension these vectors to 1.15 (xxxxx).

- (ii) Ill-conditioning of the structure model causes the message:

INDEFINITE MATRIX; THIS CASE CANCELLED.

Execution continues with the next case. The most likely cause is misplacement of the crack tip, relative to the bushing O.D. Recheck the input data to make sure that the crack tip does not extend beyond the bushing, even if a single-material lug is being analyzed. Material property errors are another probable source. Ill-conditioning may result if the bushing is too stiff, compared to the lug, or vice versa. Errors may also results from incorrect specification of orthotropic material properties.

3.6 Visual Interpretation of Output

Level contour plots are recommended as the best means of visually interpreting the output from a stress analysis case. For this purpose, a scale plan of the lug outline should be prepared and the element centroid positions marked on the plan. The stress values may then be transferred and a contour plot prepared. Plots of σ_{rr} , $\sigma_{\theta\theta}$, $\sigma_{r\theta}$ in the region around the bearing pinhole and of σ_{xx} , σ_{yy} , σ_{xy} in the shank region are recommended. The nodal displacement solution table may be used to provide a plot of the deformed structure, if desired. The output from a stress intensity analysis is best treated by means of polar plots for K_I and K_{II} . These plots are discussed in detail with examples in Section 4.

3.7 Program Status

At the date of this report, the following program options have been exercised successfully:

- (i) Stress and stress intensity analysis.
- (ii) Bearing load: tension, compression, positive shear, and negative shear.
- (iii) Cosine and uniform pressure distribution.
- (iv) Isotropic, single-material lug.
- (v) $NT = 3, 4, \text{ and } 6$.

The following options have not been exercised to date:

- (vi) Isotropic, two-material lug.
- (vii) Isotropic bushing with orthotropic lug.
- (viii) $NT > 6$.

Section 4

RESULTS OF EXAMPLE ANALYSES

Two example analyses were run to demonstrate the program. The first was limited to stress and stress intensity analysis of the hypothetical wing root attachment lug shown in Figure 9. Second, a detail similar to the aft engine support pylon truss lug in the C-5A was subjected to a more extensive analysis. Experience with the program to date, on IBM S-370/165 and S-370/168 computers, indicates that approximately 1.8 to 3.6 CPU seconds per K_I , K_{II} solution pair are required, depending upon the amount of detail in the model.

4.1 Analysis of Wing Root Attachment Lug

Figure 18 summarizes the stress distribution in the hypothetical wing lug. Stress contours for σ_{rr} , $\sigma_{\theta\theta}$, and $\sigma_{r\theta}$ are shown. A survey of the numerical data confirmed that σ_{rr} , $\sigma_{\theta\theta}$ were symmetric about the lug centerline. Hence, only half-plots are shown for those contours. The survey also indicated that $\sigma_{r\theta}$ behaved anti-symmetrically, as shown in the second part of Figure 18.

Figure 19 presents polar "butterfly" plots for K_I and K_{II} as functions of angle to the crack opening. The crack was 0.5 inches long and oriented radially. Again, the data behave symmetrically about the lug centerline (crack at 0° and 180° locations). The interpretation of these polar plots is explained in Figure 20. If the origin of the plot is identified with the center of the bearing pinhole, a radius vector through the assumed crack location may be constructed. The length of the vector between the origin and the K-plot then gives the corresponding stress intensity value.

If the crack size is small compared with the lug dimensions, there follows an intuitive hypothesis that the stress intensities ought to behave in the same manner as the uncracked structure stresses. This hypothesis can be confirmed, for the present case, by comparison of Figures 18 and 19. For a radially-oriented crack,

K_I should be influenced primarily by $\sigma_{\theta\theta}$, while K_{II} should be influenced primarily by $\sigma_{r\theta}$. Maxima of $\sigma_{\theta\theta}$ and K_I are observed to occur near $\theta = 90^\circ, 270^\circ$. Maxima of $\sigma_{r\theta}$ occur approximately at $\theta = 45^\circ, 135^\circ, 225^\circ$, and 315° , while K_{II} maxima occur approximately at $60^\circ, 120^\circ, 240^\circ$, and 300° . The apparent discrepancy between K_{II} and $\sigma_{r\theta}$ can be explained by recognizing that the crack tip actually lies near the 1.5 and 2.0 ksi stress contours. Local maxima for $\sigma_{r\theta}$ in those regions are less sharply defined.

4.2 Analysis of Engine Pylon Truss Lug

Figure 21 is a scale plot of the structure model used to analyze a detail similar to the C-5A engine pylon aft truss lug. The actual lug has two tongues to place the bearing pin in double shear. It can be reasonably assumed that the load transferred into the engine pylon at this point is borne equally by both tongues. Hence, the lug program has been used to analyze one tongue. The model is 0.19 inch thick, with:

$$\begin{array}{ll} D_I = 1.75 \text{ inches} & D_B = 2.35 \text{ inches} \\ H = 10.5 \text{ inches} & W = 3.5 \text{ inches} \end{array}$$

A 0.15-inch long crack was assumed, with radial orientation. Material properties for high-strength steel alloys were used:

$$E = 30 \times 10^6 \text{ psi} \quad \nu = 0.295$$

The "bushing" O.D. was chosen merely to locate the crack tip at the middle of the bushing region. Models were run with 24 elements ($NT = 3$, "coarse mesh") and 32 elements ($NT = 4$, "fine mesh") around the bearing pinhole. The fine mesh model is shown in Figure 21. All runs were made with a 1,000-pound bearing load, as a standard for plotting the results.

Figure 22 summarizes the stress distribution near the hole, as obtained from a fine mesh model of the uncracked structure, with a cosine bearing pressure distribution. The symmetries discussed in Subsection 4.1 were observed again. Three additional checks were made to assure that the model accurately reflects the stress

gradients caused by the lug geometry. First, in a typical section through the shank, the tension stress σ_{xx} was found to be uniform and statically equivalent to the bearing load, to better than one percent accuracy, for both models. Second, a section was taken through the bearing pinhole center ($\theta = 90^\circ, 270^\circ$) and $\sigma_{\theta\theta}$ was plotted. The radial variation of $\sigma_{\theta\theta}$ was found to agree generally with Timoshenko's classical solution for an eye bolt under tension bearing [17]. Also, numerical evaluation of $T/\sigma_{\theta\theta} dr$ gave the bearing load, with 1.7 percent error for the coarse mesh and 1.4 percent error for the fine mesh. Finally, the solution for σ_{rr} was compared with the bearing pressure distribution. The peak value of the bearing pressure is given by $p_o = P/\pi D_I T$, where P is the bearing load. For the present case, $p_o = 3.83$ ksi and acts at $\theta = 0^\circ$. The two elements with centroid locations nearest to $r = D_I/2$, $\theta = 0^\circ$ were found to have $\sigma_{rr} = 3.5$ ksi, and the radial stress could be extrapolated to a value close to p_o at the peak point. Based on these results and the measured performance of the PCRK59 element (Subsection 2.2), the fine mesh model was accepted as giving a converged solution for K_I , having a cumulative error of 5 percent.

Butterfly plots for K_I and K_{II} are shown in Figure 23. Again, the stress intensities behave symmetrically to better than 1 percent accuracy for both models, and K_I follows $\sigma_{\theta\theta}$, while K_{II} follows $\sigma_{r\theta}$. The data for K_I , shown in the upper half of the figure, demonstrate that convergence has been obtained. The data for K_{II} , in the lower half of the figure, indicate that additional refinement of the mesh might be required to demonstrate Mode II stress intensity convergence. However, since the K_{II} values are generally smaller than K_I , and since they tend to decrease as the solution converges, no further refinements were made. The coarse model contained 408 degrees of freedom and took 48 CPU seconds to compute a complete set of 24 pairs of K_I and K_{II} solutions. The fine model contained 608 degrees of freedom and took 102 CPU seconds to compute 32 solutions.

The length of the lug detail was reduced from 10.5 inches to 7.0 inches for the remaining analyses, to eliminate superfluous elements in the shank and thus reduce computation costs. Fine

mesh models (and a few "very fine" models) were analyzed in the remaining series. The shortened lug fine mesh model is illustrated by Figure 24.

The stress intensity analysis for cosine tension bearing was repeated to assess the influence of the change in shank length. Figure 25 compares the K_I and K_{II} butterfly plots from Figure 23 with corresponding plots for the shortened lug. A slight increase in stress intensities with decrease in shank length can be observed. Figure 26 compares butterfly plots for the 7-inch lug under cosine and uniform bearing. Three significant differences can be observed:

- (i) The increased ability of a uniform bearing pressure to spread the part outward changes the hoop stress from compression to tension at $\theta = 0^\circ$. Compare the uncracked structure stress contours for cosine bearing (Figure 22) with the contours for uniform bearing, shown in Figure 27.
- (ii) The maximum K_I value changes from 5 ksi $\sqrt{\text{in.}}$ at $\theta = 85^\circ$ (cosine bearing) to about 4.7 ksi $\sqrt{\text{in.}}$ at $\theta = 107^\circ$ (uniform bearing).
- (iii) Mode II stress intensities are lower for uniform bearing.

The third series of runs analyzed the case of positive shear bearing. Figure 28 illustrates the stress contours obtained for shear bearing with a cosine distribution. The behavior of σ_{rr} near the bearing pressure peak (now at $\theta = 90^\circ$) is similar to the tension bearing case (compare with Figure 22). The Cartesian stress components in the shank region were surveyed to provide additional equilibrium checks. Figure 29 compares the finite element stress distributions for σ_{XX} , σ_{XY} through a typical shank section and for σ_{XX} axially, with engineering beam theory calculations:

$$\sigma_{XX} = - \frac{M(X)Y}{I} \qquad \sigma_{XY} = \frac{3V(X)}{2A} \left[1 - \left(\frac{2Y}{W} \right)^2 \right] \qquad (25)$$

where

$M(X)$ = Section bending moment at X

$V(X)$ = Section shear at X

I = Section moment of inertia = $TW^3/12$

A = Section area = TW

It is evident from the figure that the finite element results are within 1 or 2 percent of engineering beam theory. The only exception is the axial behavior of σ_{XX} which exhibits some stress concentration effects:

- (i) Due to the cantilever restraints, as the left end of the shank is approached.
- (ii) Due to the influence of the hole, as the shank/ear interface is approached.

Based on these results, the fine mesh model was judged to be capable of giving stress intensities for shear bearing which are comparable to the tension bearing results (5 percent error).

Figures 30 and 31 present K_I and K_{II} butterfly plots for cosine and uniform pressure distributions, respectively. Data for a "very fine" model ($NT = 6$, 48 elements around the hole) as well as for the fine mesh model, are shown in Figure 31. The refined model was run to improve the fairing of the curves, after plots of the fine mesh model were seen to have large gaps between K_I data points. The refined model data indicate that the fine mesh has not quite converged the K_I solutions. Two interesting features are illustrated by these plots. First, the stress intensity maxima and minima no longer coincide with the stress distribution. Apparently, even a small crack is sufficient to change the stress distribution significantly when the bearing load is shear. Second, the significant difference between cosine and uniform pressure now occurs at the K_I maxima, which are about 10 percent larger for uniform pressure. This arises from the fact that the K_I maxima are located near and nearly opposite to the bearing load line of action.

A fourth series of analyses treated the case of compression bearing, using only the fine mesh model. Both the stresses and stress intensities were found to behave symmetrically, similar to the case of tension bearing. Equilibrium checks and stress contour plots have been omitted, in view of the results already presented. Figures 32 and 33 show K_I and K_{II} butterfly plots for compression bearing with cosine and uniform distribution, respectively. The most interesting feature is the extreme sensitivity to load distribution when the crack is at or opposite to the load center. The Mode I stress intensity for uniform bearing increases by factors of 2 at the first location and 4 at the second. This extreme sensitivity results from the high hoop stresses which are present in these regions.

4.3 Example Application

To provide an example of how the butterfly plots may be applied to structural integrity verification analysis, the following data have been abstracted from load calculations for the original C-5A engine pylon truss design [22]:

<u>Load Condition</u>	<u>Tension (Compression)</u>	<u>Shear</u>
"Maximum Compression" (MC)	-221×10^3 lb.	-340 lb.
"Maximum Tension" (MT)	148×10^3 lb.	220 lb.

The values in the above table represent total load transferred through the attachment lug, and must be divided by 2 to obtain the loads per tongue. Since shear bearing can obviously be ignored for the above conditions, there results:

Condition MC: 110.5×10^3 lb. Compression Bearing

Condition MT: 74×10^3 lb. Tension Bearing

Assuming that a cosine pressure distribution is representative, the following calculations can be made for 0.15-inch cracks assumed to be located at 0°, 45°, 90°, and 180°:

Crack Location	Condition MC (K values in ksi√in.)	Condition MT (K values in ksi√in.)
0°	$K_I \approx 0.4 \times 110.5 = 44.2$ $K_{II} = 0$	$K_I = K_{II} \approx 0$
45°	$K_I \approx 0.3 \times 110.5 = 33.2$ $K_{II} \approx 0$	$K_I \approx 2.6 \times 74 = 192.4$ $K_{II} \approx 1.25 \times 74 = 92.5$
90°	$K_I = K_{II} = 0$	$K_I \approx 5 \times 74 = 370$ $K_{II} \approx 0.2 \times 74 = 14.8$
180°	$K_I \approx 1.63 \times 110.5 = 180.1$ $K_{II} = 0$	$K_I = K_{II} \approx 0$

"Unit" K values are read from Figure 26 for Condition MT and from Figure 32 for Condition MC. The actual values are then computed by using the actual load to scale the unit values.

Potential fracture sites may be assessed by comparing K_I with K_{IC} for a proposed lug material. Since high strength steel alloys have fracture toughness generally below 100 ksi √in., the above data indicate that a 0.15-inch crack is longer than critical size if the crack is located at 45°, 90°, or 180°. If a criterion that 0.15-inch cracks be less than critical is to be met, the designer might do this by increasing the lug thickness. Since the numerical data result from a linear analysis, the design can be scaled. For example, a revised thickness

$$T' = \frac{370}{K_{IC}} \times T = \frac{370}{50} \times 0.19 \approx 1.41 \text{ in.} \quad (26)$$

can be calculated, assuming that protection against a 0.15-inch crack at 90°, in a material with $K_{IC} = 50$ ksi √in., is required. At other points; e.g., $\theta = 45^\circ$ (Condition MT), K_I and K_{II} are comparable, and interaction formulas such as:

$$\left(\frac{K_I}{K_{IC}}\right)^2 + \left(\frac{K_{II}}{K_{IIC}}\right)^2 \leq 1 \quad (27)$$

may be used to assess structural integrity.

Section 5

CONCLUSIONS

A finite-element analysis program for computation of Mode I and Mode II stress intensity factors in attachment lug details has been presented. Since the program is based on an assumed-stress hybrid crack element, relatively crude structure models can be used. Performance tests of the crack element and the lug program have indicated that K_I and K_{II} solutions can be obtained to ± 5 percent accuracy, for 1.8 to 3.6 CPU seconds per solution pair on current-generation large computers.

A series of demonstration examples, involving a lug detail similar to the C-5A engine pylon aft truss attachment lug, served to illustrate a number of important features of the K solutions. With the crack size held at 0.15 inch and the crack orientation kept radial, parametric analyses were conducted for K_I and K_{II} with the lug subjected to tension, shear and compression bearing forces. In each case, data were obtained for both a cosine and a uniform pressure distribution, to represent possible extremes of load transfer across the bearing surface. The parametric capability of the program was used to compute for each case a number of K_I and K_{II} values corresponding to location of the crack at various positions around the bearing pinhole. Polar plots of K_I and K_{II} versus angle to the crack location were presented to provide a concise picture of the parametric behavior.

The following specific conclusions can be drawn from the results of the analysis. First, uniform bearing pressure has more tendency than cosine pressure to spread the lug apart, and this is reflected by increased K_I values. This effect interacts with the relation between the crack location and the line of action of the bearing load. The most significant sensitivity to pressure distribution occurs when a K_I maxima coincides with or is close to the line of action of the load, or when a maximum lies opposite to the

load line. Second, the most critical locations for a given crack often lie in unexpected places or correspond to unexpected load conditions. For example, cracks at $\pm 90^\circ$ to the lug axis appear to be most critical in tension bearing. However, cracks at $\pm 45^\circ$ may actually be the most critical if the lug material happens to have a low Mode II fracture toughness. A significant Mode I stress intensity value for a crack at 180° , under compression bearing, is another unexpected result. Finally, the maxima and minima of K_I and K_{II} sometimes tend to follow local maxima and minima of the stress distribution in an equivalent uncracked structure, if the crack is small compared to the structure detail dimensions. However, the coincidence of maxima and minima occurs only for some load conditions, while significant discrepancies occur under other load conditions. One is, therefore, led to conclude that a stress analysis of an uncracked structure does not always provide a good map of where to expect the most critical stress intensities, even for small cracks.

REFERENCES

1. Campbell, J. E., et al., "Damage Tolerant Design Handbook", Metals and Ceramics Information Center, Battelle Columbus Laboratories, 505 King Avenue, Columbus, Ohio, 1972.
2. Matthews, W. T., "Plane Strain Fracture Toughness (K_{IC}) Data Handbook for Metals", Army Materials and Mechanics Research Center, Watertown, Massachusetts 02172, AMMRC MS 73-6, December 1973.
3. Anon., "Airplane Damage Tolerance Design Requirements", MIL-A-83444, U.S. Air Force Aeronautical Systems Division, Wright-Patterson AFB, Ohio 45433, June 1974.
4. Bowie, O. L., J. Appl. Mech., Vol. 31, pp. 208-212 (1964).
5. Bowie, O. L. and Neal, D. M., Int. J. Fracture Mech., Vol. 6, pp. 199-206 (1970).
6. Bowie, O. L., Freese, C. E. and Neal, D. M., "Solution of Plane Problems of Elasticity Utilizing Partitioning Concepts", ASME Paper No. 73-APM-C, 1973.
7. Tada, H., Paris, P. C., and Irwin, G. R., The Stress Analysis of Cracks Handbook, DEL Research Corporation, Hellertown, Pennsylvania, 1973.
8. Pian, T. H. H., AIAA J., Vol. 2, pp. 1333-1336 (1964).
9. Tong, P. and Pian, T. H. H., Int. J. Solids Struc., Vol. 9, pp. 313-321 (1973).
10. Luk, C. H., "Assumed Stress Hybrid Finite Element Methodology for Fracture Mechanics and Elastic-Plastic Analysis", Aeroelastic and Structures Research Laboratory, MIT, ASRL TR 170-1, December 1972.
11. Tong, P., Pian, T. H. H. and Lasry, S. J., Int. J. Num. Meth. Eng., Vol. 7, pp. 297-308 (1973).
12. Lasry, S. J., "Derivation of Crack Element Stiffness Matrix by the Complex Variable Approach", Aeroelastic and Structures Research Laboratory, MIT, ASRL TR 170-2, AFOSR-TR-73-1602, February 1973.
13. Zienkiewicz, O. C. and Cheung, Y. K., The Finite Element Method in Structural and Continuum Mechanics, McGraw-Hill, 1967.

14. Abramowitz, M. and Stegun, I. A. (ed.), Handbook of Mathematical Functions, National Bureau of Standards, U.S. Department of Commerce, Ninth Ed., November 1970.
15. Desai, C. S. and Abel, J. F., Introduction to the Finite Element Method, Van Nostrand Reinhold Company, 1970.
16. Orringer, O., "FEABL (Finite Element Analysis Basic Library) Documentation of Sample Program for Export Version", Aeroelastic and Structures Research Laboratory, MIT, ASRL TM 162-3-4, February 1974.
17. Timoshenko, S. and Goodier, J. N., Theory of Elasticity, McGraw-Hill, 1961.
18. Washizu, K., Variational Methods in Elasticity and Plasticity, Pergamon Press, 1968.
19. Lin, K. Y., Tong, P. and Orringer, O., "Effect of Shape and Size on Hybrid Crack-Containing Finite Elements", submitted for presentation at ASME Pressure Vessels and Piping Conference, San Francisco, California, June 1975.
20. Orringer, O. and French, S. E., "FEABL (Finite Element Analysis Basic Library) User's Guide", Aeroelastic and Structures Research Laboratory, MIT, ASRL TR 162-3, AFOSR-TR-72-2228, August 1972.
21. Orringer, O. and French, S. E., "FEABL (Finite Element Analysis Basic Library) Version 2/Release 2", Aeroelastic and Structures Research Laboratory, MIT, ASRL TM 162-3-3, February 1974.
22. Neilson, J. A., Shockley, E. J. and Dallas, C. H., "C-5A Pylon Evaluation and Redesign Recommendations", Lockheed-Georgia Aircraft Company, Marietta, Georgia, Report No. SRD 72-21-775, p. 29.

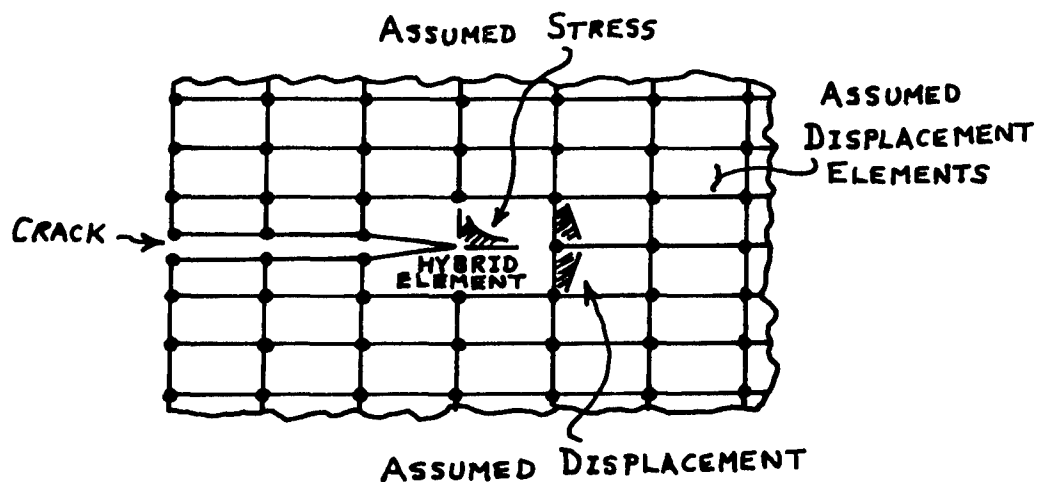


FIG. 1 COMBINATION OF ASSUMED-DISPLACEMENT ELEMENTS WITH HYBRID CRACK-CONTAINING ELEMENT

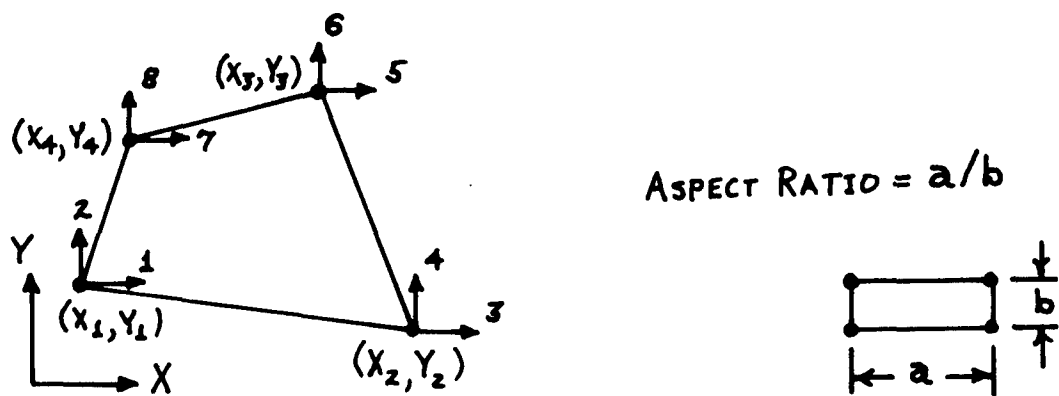


FIG. 2 CONVENTIONS FOR ASRL QUAD4 ASSUMED-DISPLACEMENT ELEMENT

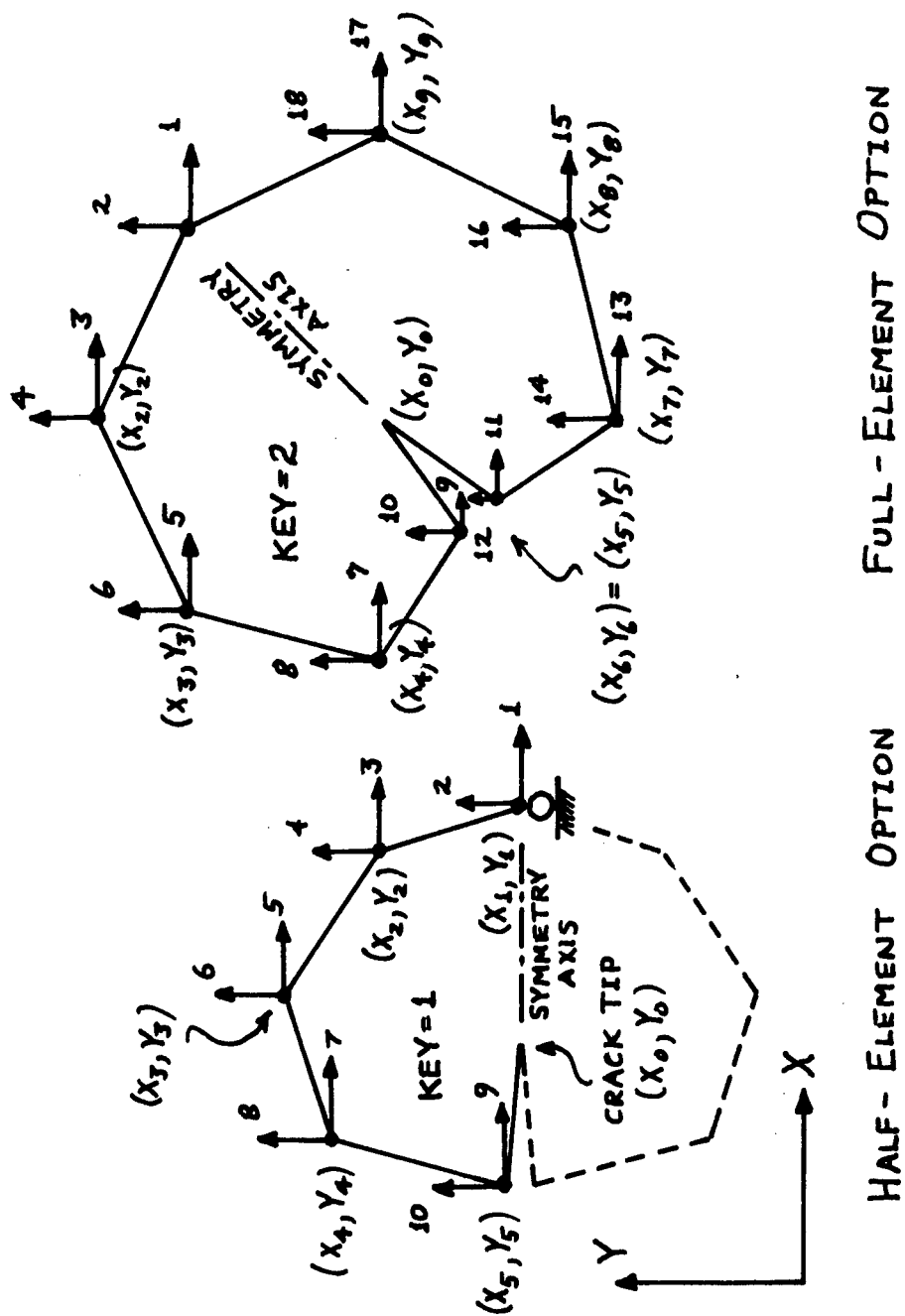
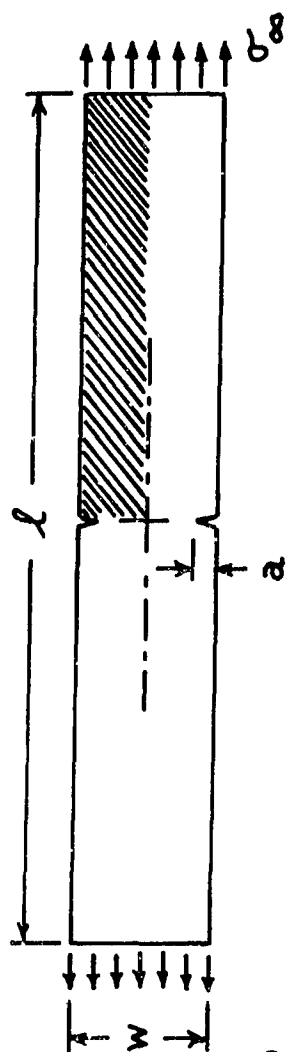
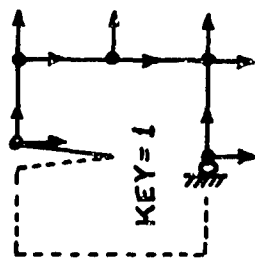


FIG. 3 ASRL PCRK59 HYBRID CRACK-CONTAINING ELEMENT

LONG PLATE WITH SYMMETRICAL EDGE CRACKS



PCRK59
ELEMENT



FINITE ELEMENT MODEL OF SHADED REGION

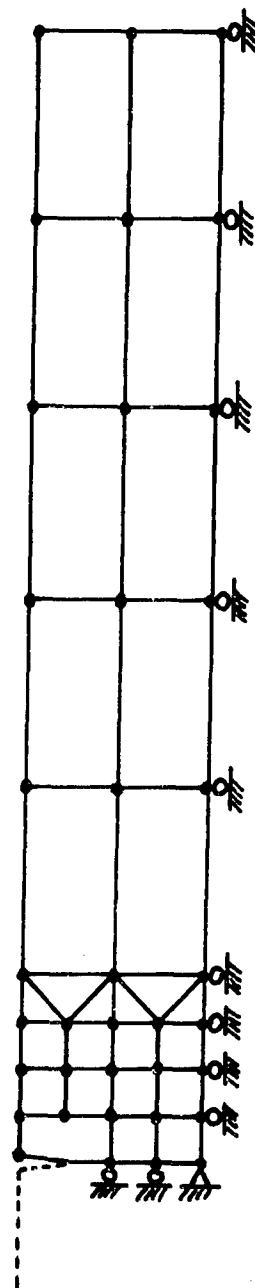


FIG. 4 APPLICATION OF PCRK59 ELEMENT TO SYMMETRIC ANALYSES

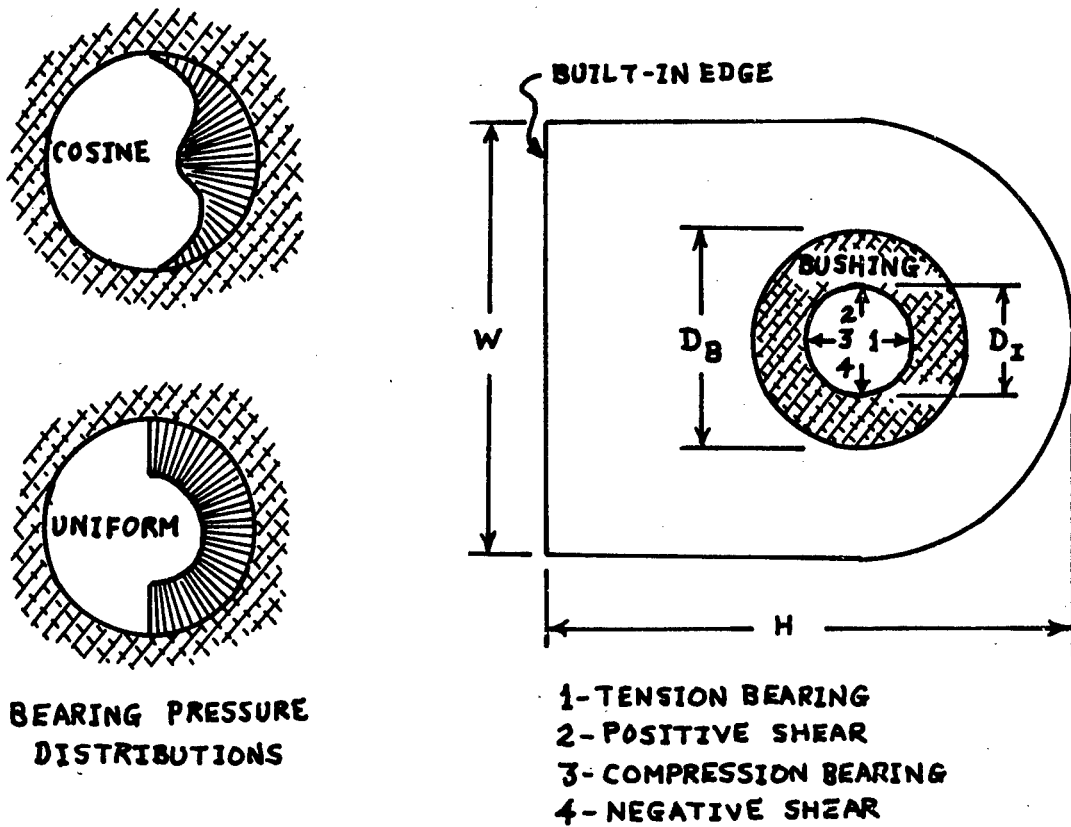


FIG. 5 ATTACHMENT LUG DETAIL

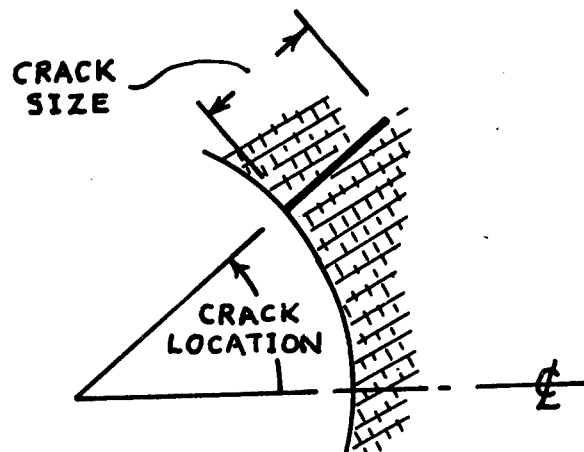


FIG. 6 CRACK PARAMETERS

AEROELASTIC AND STRUCTURES RESEARCH LABORATORY		ENGINEER	
JOB TITLE		ORRINGER	
ATTACHMENT LUG PROGRAM - INPUT CONVENTIONS			
JOB NO.	PROGRAMMER	DATE	SHEET
	ORRINGER / FRENCH	9 DEC 74	1 OF 1
CARD #	1	NCASES(15) = TOTAL # CASES FOR THE RUN	
2		TTITLE(20A4) = ANY ALPHANUMERIC TITLE FOR CASE	
3		IANL * LOAD * MODE * NT * (415) IANL = ANALYSIS OPTION LOAD = LOAD OPTION MODE = 1 (ISOTROPIC) OR 2 (ORTHOTROPIC) NT = # ELEMENTS PER 45° ARC	
4		DI * DB * W * H * TT * CSIZE * (6E10.0) DI = BEARING PIN HOLE I.D. DB = BUSHING O.D. W = LUG WIDTH H = TOTAL LUG LENGTH TT = LUG THICKNESS CSIZE = CRACK LENGTH	
5		E * V * (2E10.0) BUSHING PROPERTIES: E = YOUNG'S MODULUS V = POISSON'S RATIO	
6		E * ET * GLT * TH * (5E10.0) FOR ORTHOTROPIC LUG (MODE=2) EL = LONGITUDINAL MODULUS ETL = CROSS-COUPLING MODULUS ET = TRANSVERSE MODULUS GLT = SHEAR MODULUS TH = ANGLE FROM LUG Q TO MATERIAL "L" AXIS (DEG, POSITIVE CCW)	
7		TENSN * SHEAR * (2E10.0) TENSN = TENSION (POSITIVE) OR COMPRESSION (NEGATIVE) BEARING FORCE SHEAR = POSITIVE OR NEGATIVE SHEAR BEARING FORCE	
NOTE: REPEAT CARD STACK #2 THRU #7 FOR EACH CASE			

FIG. 7 PROGRAM LUG INPUT CONVENTIONS

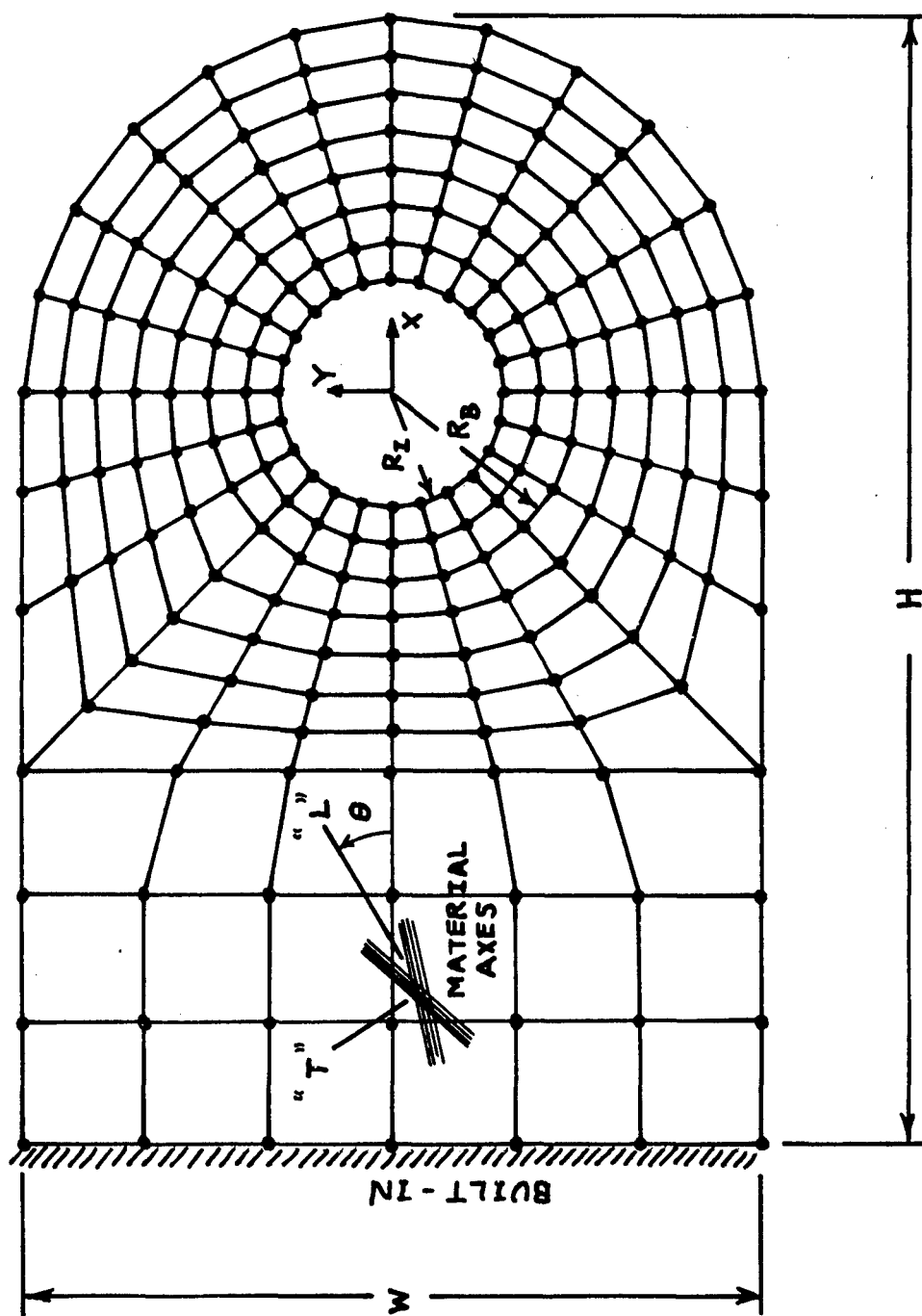


FIG. 8 FINITE ELEMENT MESH FOR $NT = 3$

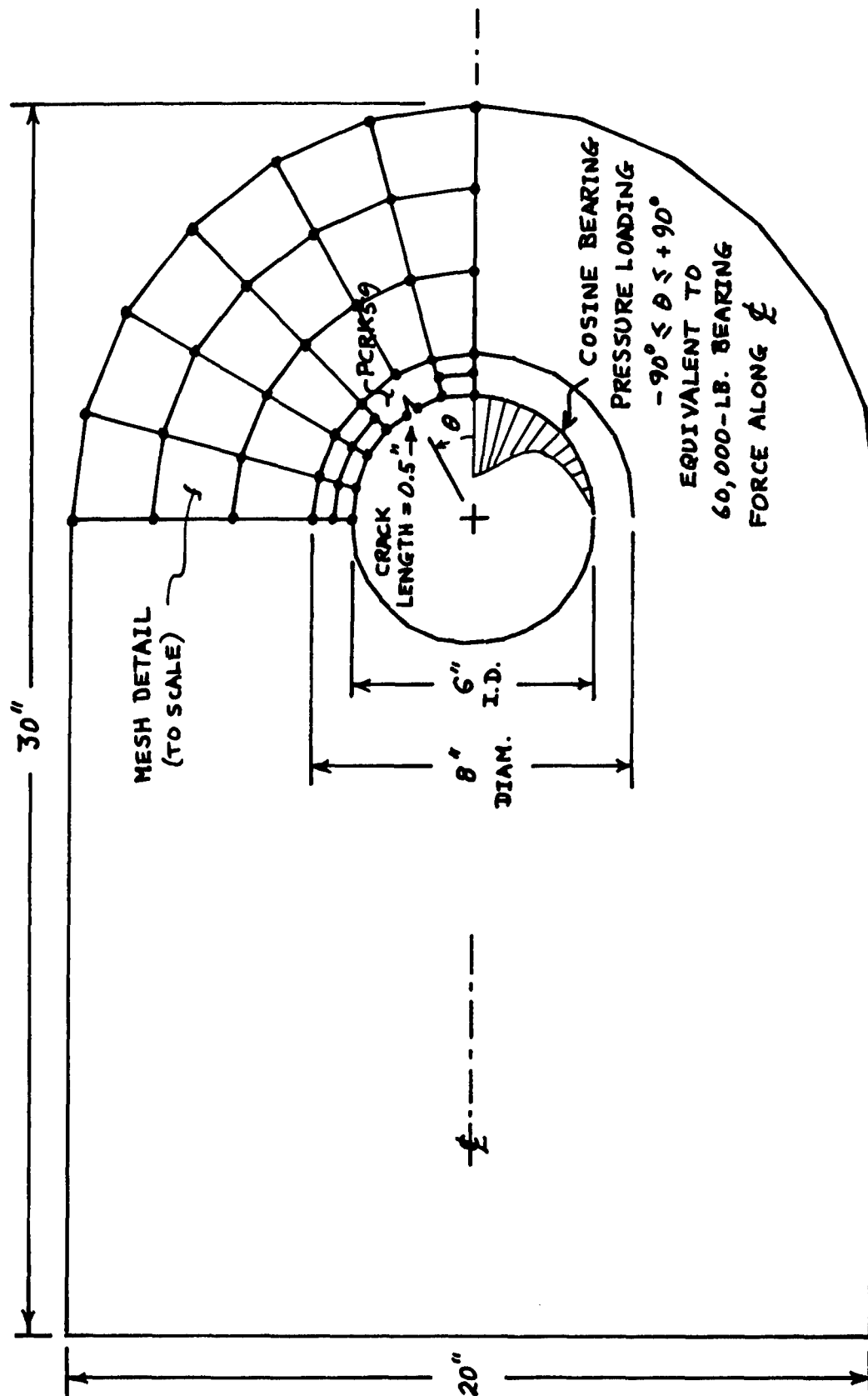


FIG. 9 HYPOTHETICAL WING ROOT ATTACHMENT LUG

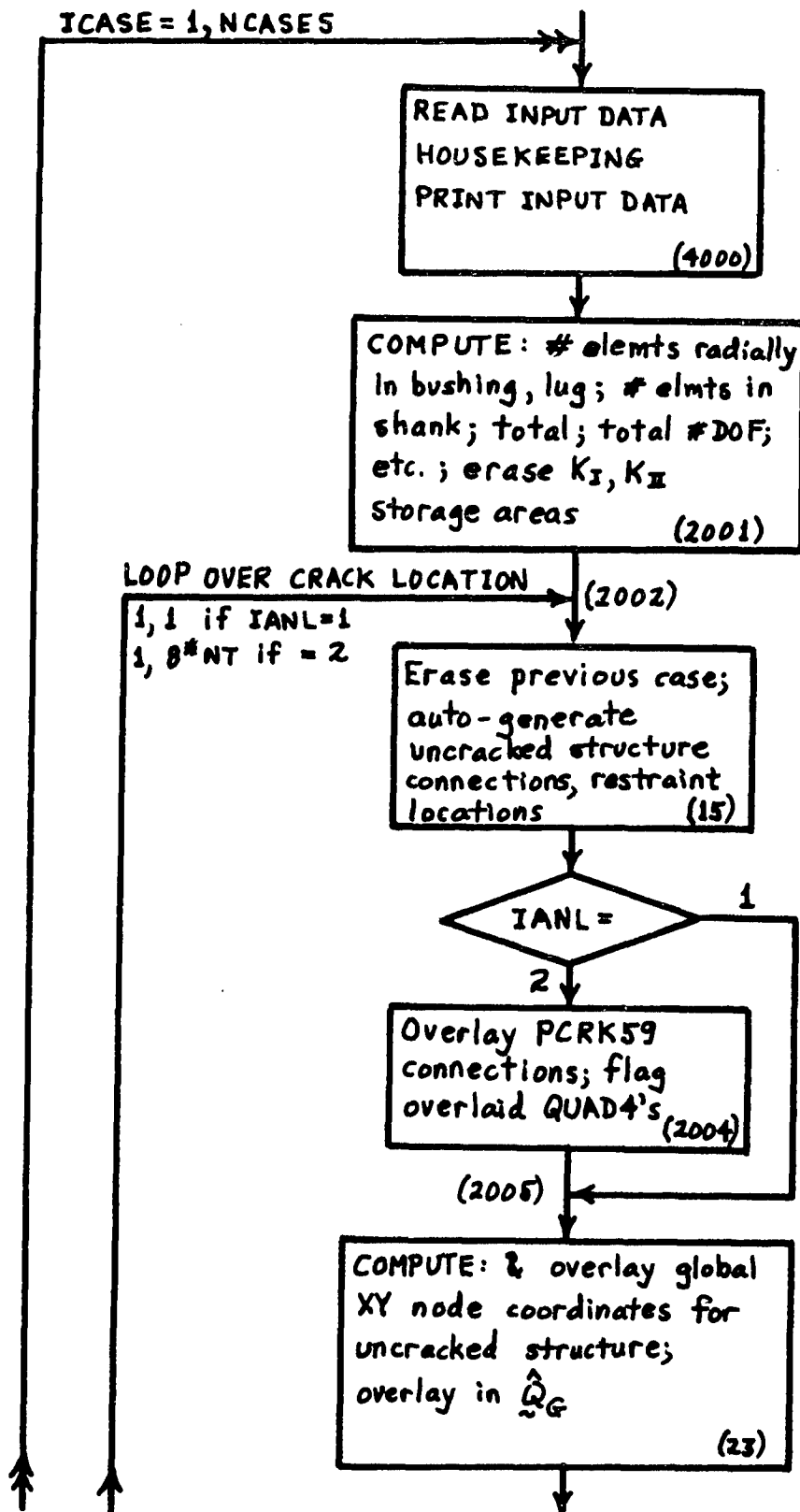


FIG. 11 PROGRAM LUG FLOW CHART

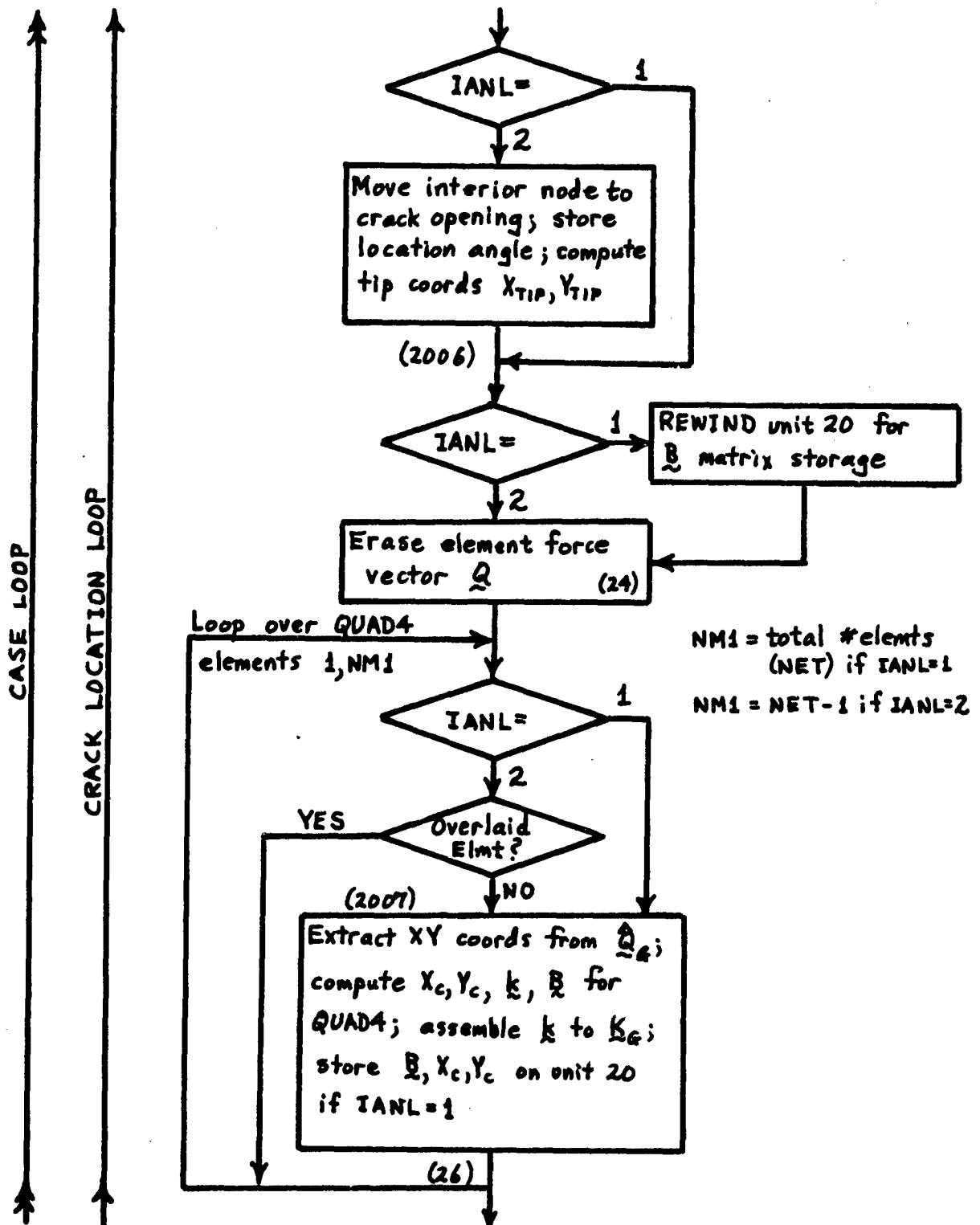


FIG. 11 (CONTINUED)

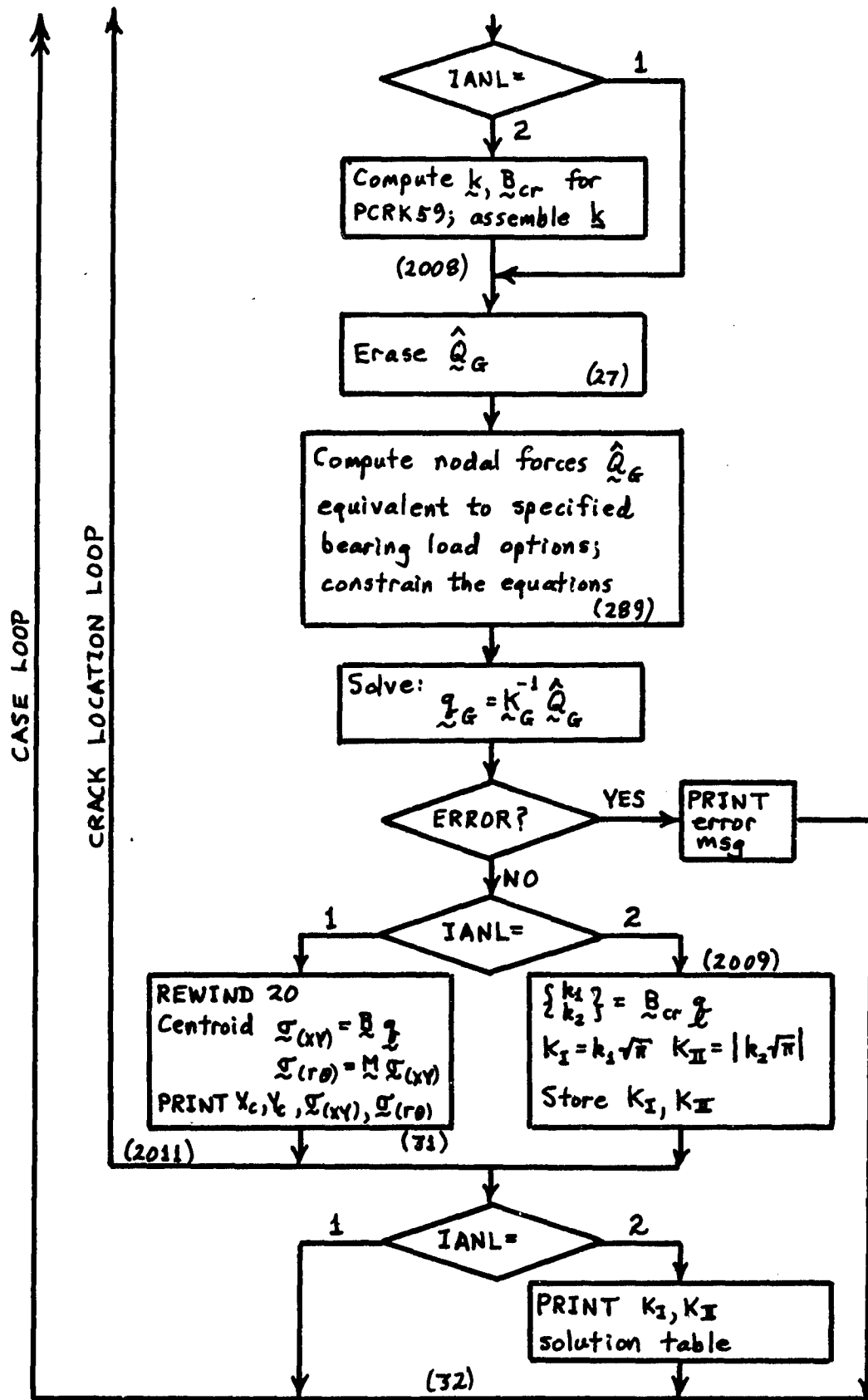


FIG. 11 (CONCLUDED)

```

CASE 36: LUG PROGRAM STRESS INTENSITY ANALYSIS

ANALYSIS OPTION= 2; LCAD OPTION= 2

MODE= 1 (1-ISOTROPIC, 2-CRTHCTEFC LUG)
TOTAL OF 32 ELEMENTS AROUND PIN HOLE
HOLE I.D.= 0.200E+01 BUSHING O.D.= 0.300E+01 LUG WIDTH= 0.400E+01 LUG LENGTH= 0.700E+01 THICKNESS= 0.100E+01

CRACK LENGTH= 0.200E+00; DIRECTION= 0.0

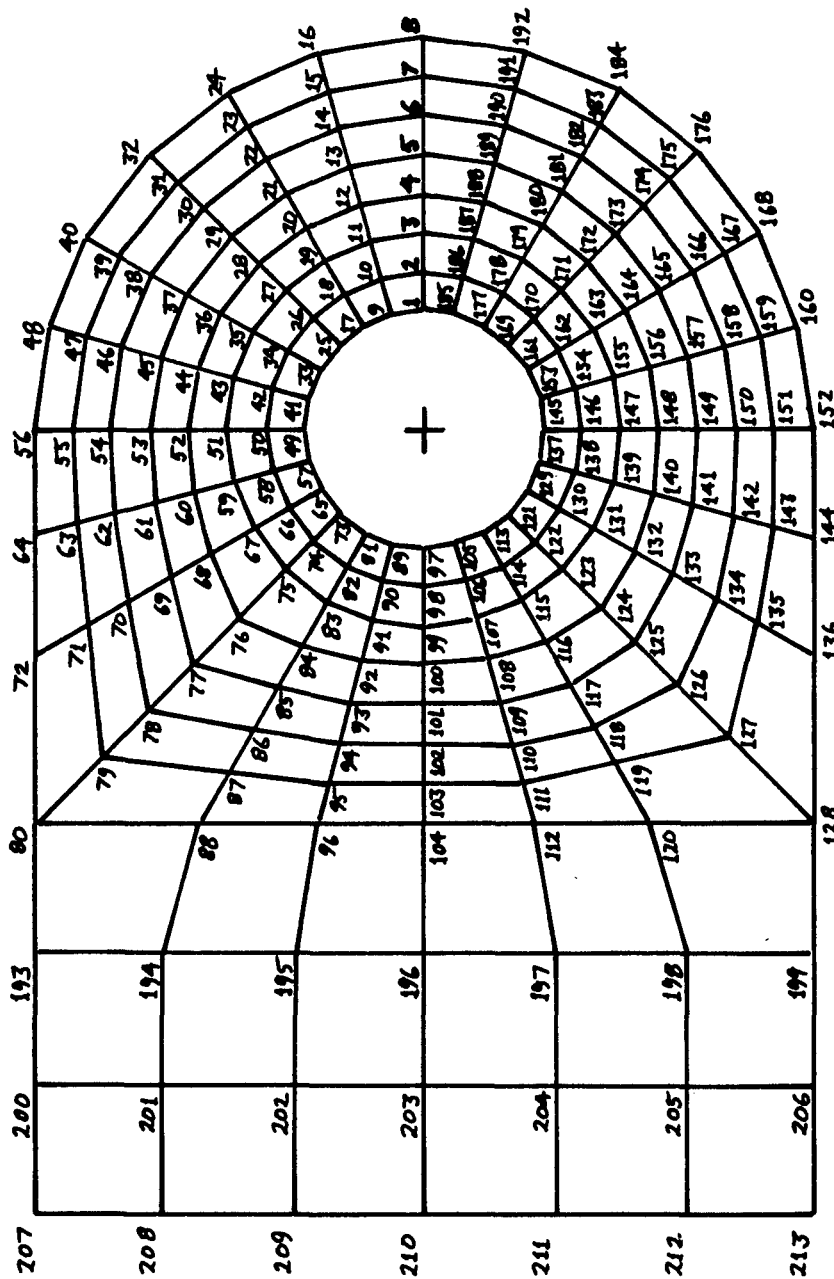
BUSHING MATERIAL: E= 0.100E+08 NU= 0.300E+00

ISOTROPIC LUG: E= 0.100E+08 NU= 0.300E+00

APPLIED TENSION= 0.100E+04 LB. AND SHEAR= 0.0 LB.

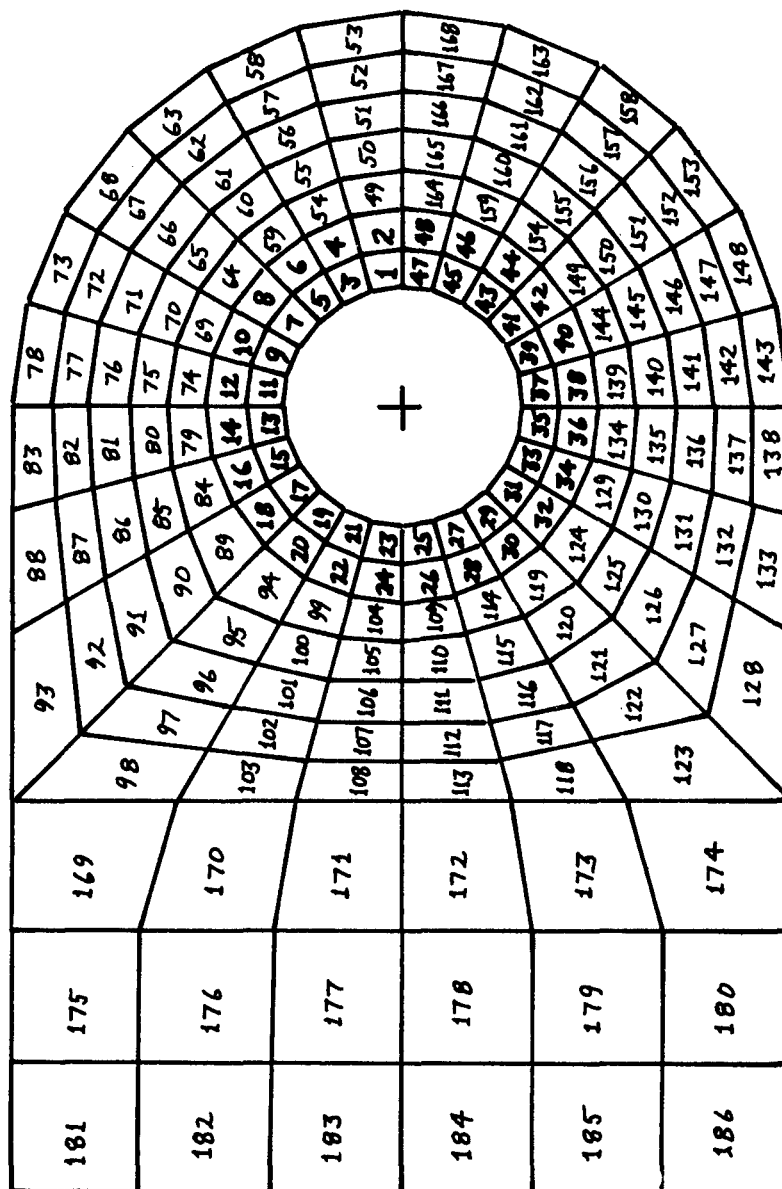
```

FIG. 12 PRINTOUT OF INPUT DATA



(a) Node Numbering Diagram

FIG. 13 NUMBERING CONVENTIONS ILLUSTRATED FOR SAMPLE MESH SHOWN IN FIG. 8



(b) Element Numbering Diagram

FIG. 13 (CONCLUDED)

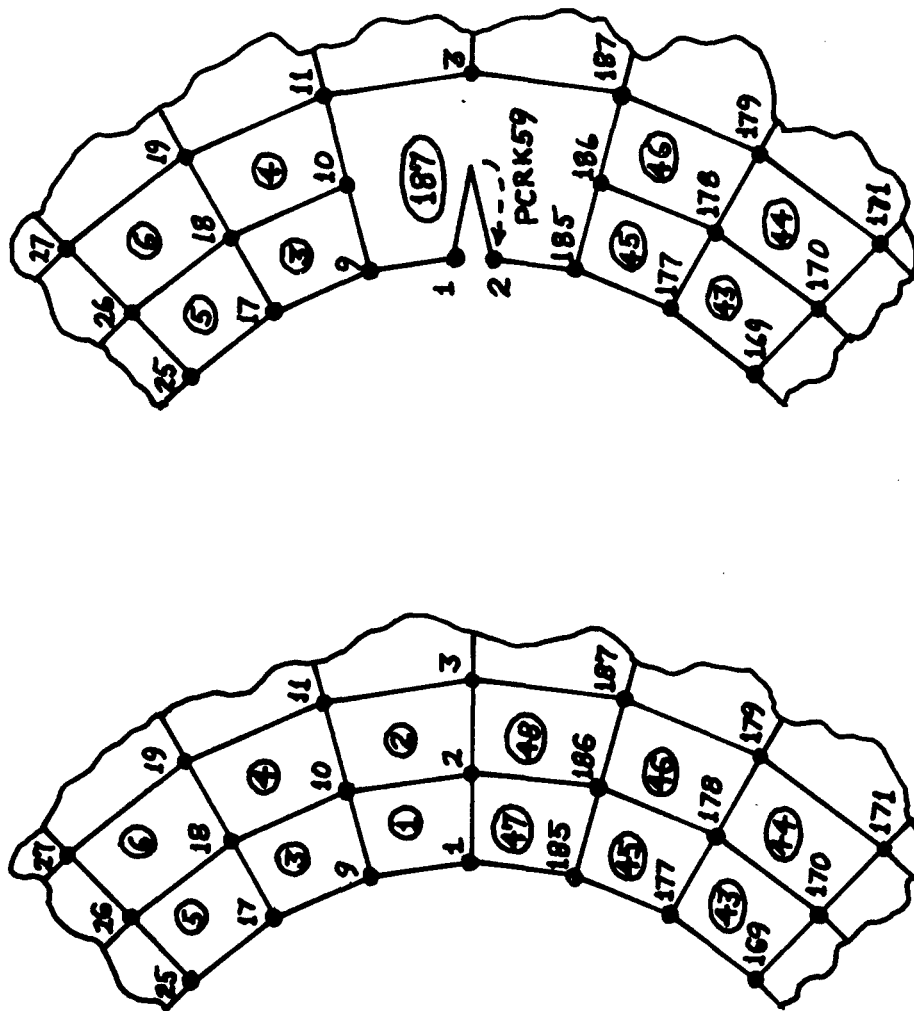


FIG. 14 OVERLAY FOR STRESS INTENSITY ANALYSIS

CASE 11 CASE 1		11 DECEMBER 1974	
ANALYSIS OPTION= 11 LOAD OPTION= 2			
MODE= 1 11-ISOTROPIC, 2-ORTHOTROPIC LUG			
TOTAL OF 32 ELEMENTS AROUND PIN HOLE			
HOLE I.D.= 0.135E+01 BUSHING O.D.= 0.235E+01 LUG WIDTH= 0.350E+01 LUG LENGTH= 0.700E+01 THICKNESS= 0.190E+00			
BUSHING MATERIAL E= 0.300E+08 NU= 0.255E+00			
ISOTROPIC LUG E= 0.300E+08 NU= 0.255E+00			
APPLIED TENSION= 0.100E+04 LB. AND SHEAR= 0.0 LB.			
SIMULQ ENTRY POINT			
PREScribed FORCE/DISPLACEMENT VECTOR:			
ROW	1	2	3
VALUE	0.987E+02	-0.124E-03	0.0
ROW	11	12	13
VALUE	0.963E+02	0.192E+02	0.0
ROW	21	22	23
VALUE	0.907E+02	0.376E+02	0.0
ROW	31	32	33
VALUE	0.816E+02	0.545E+02	0.0
ROW	41	42	43
VALUE	0.694E+02	0.694E+02	0.0
ROW	51	52	53
VALUE	0.545E+02	0.816E+02	0.0
ROW	61	62	63
VALUE	0.376E+02	0.907E+02	0.0
ROW	71	72	73
VALUE	0.192E+02	0.963E+02	0.0
ROW	81	82	83
VALUE	0.0	0.491E+02	0.0
ROW	91	92	93
VALUE	0.0	0.0	0.0
ROW	101	102	103
VALUE	0.0	0.0	0.0
ROW	111	112	113
VALUE	0.0	0.0	0.0
ROW	121	122	123
VALUE	0.0	0.0	0.0
ROW	131	132	133
VALUE	0.0	0.0	0.0
ROW	141	142	143
VALUE	0.0	0.0	0.0
ROW	151	152	153
VALUE	0.0	0.0	0.0
ROW	161	162	163
VALUE	0.0	0.0	0.0
ROW	171	172	173
VALUE	0.0	0.0	0.0
ROW	181	182	183
VALUE	0.0	0.0	0.0
ROW	191	192	193
VALUE	0.0	0.0	0.0
ROW	201	202	203
VALUE	0.0	0.0	0.0
ROW	211	212	213
VALUE	0.0	0.0	0.0
ROW	221	222	223
VALUE	0.0	0.0	0.0
ROW	231	232	233
VALUE	0.0	0.0	0.0
ROW	241	242	243
VALUE	0.0	0.0	0.0
ROW	251	252	253
VALUE	0.0	0.0	0.0
ROW	261	262	263
VALUE	0.0	0.0	0.0
ROW	271	272	273
VALUE	0.0	0.0	0.0
ROW	281	282	283
VALUE	0.0	0.0	0.0
ROW	291	292	293
VALUE	0.0	0.0	0.0
ROW	301	302	303
VALUE	0.0	0.0	0.0
ROW	311	312	313
VALUE	0.0	0.0	0.0
ROW	321	322	323
VALUE	0.0	0.0	0.0
ROW	331	332	333
VALUE	0.0	0.0	0.0
ROW	341	342	343
VALUE	0.0	0.0	0.0
ROW	351	352	353
VALUE	0.0	0.0	0.0
ROW	361	362	363
VALUE	0.0	0.0	0.0
ROW	371	372	373
VALUE	0.0	0.0	0.0
ROW	381	382	383
VALUE	0.0	0.0	0.0
ROW	391	392	393
VALUE	0.0	0.0	0.0
ROW	401	402	403
VALUE	0.0	0.0	0.0
ROW	411	412	413
VALUE	0.0	0.0	0.0
ROW	421	422	423
VALUE	0.0	0.0	0.0
ROW	431	432	433
VALUE	0.0	0.0	0.0
ROW	441	442	443
VALUE	0.0	0.0	0.0
ROW	451	452	453
VALUE	0.0	0.0	0.0
ROW	461	462	463
VALUE	0.0	0.0	0.0
ROW	471	472	473
VALUE	0.0	0.0	0.0
ROW	481	482	483
VALUE	0.0	0.0	0.0
ROW	491	492	493
VALUE	0.0	0.0	0.0
ROW	501	502	503
VALUE	0.0	0.0	0.0
ROW	511	512	513
VALUE	0.0	0.0	0.0
ROW	521	522	523
VALUE	0.0	0.0	0.0
ROW	531	532	533
VALUE	0.0	0.0	0.0
ROW	541	542	543
VALUE	0.0	0.0	0.0
ROW	551	552	553
VALUE	0.0	0.0	0.0
ROW	561	562	563
VALUE	0.0	0.0	0.0
ROW	571	572	573
VALUE	0.0	0.0	0.0
ROW	581	582	583
VALUE	0.0	0.0	0.0
ROW	591	592	593
VALUE	0.0	0.0	0.0
ROW	601	602	603
VALUE	0.0	0.0	0.0
ROW	611	612	613
VALUE	0.0	0.0	0.0
ROW	621	622	623
VALUE	0.0	0.0	0.0
ROW	631	632	633
VALUE	0.0	0.0	0.0
ROW	641	642	643
VALUE	0.0	0.0	0.0
ROW	651	652	653
VALUE	0.0	0.0	0.0
ROW	661	662	663
VALUE	0.0	0.0	0.0
ROW	671	672	673
VALUE	0.0	0.0	0.0
ROW	681	682	683
VALUE	0.0	0.0	0.0
ROW	691	692	693
VALUE	0.0	0.0	0.0
ROW	701	702	703
VALUE	0.0	0.0	0.0
ROW	711	712	713
VALUE	0.0	0.0	0.0
ROW	721	722	723
VALUE	0.0	0.0	0.0
ROW	731	732	733
VALUE	0.0	0.0	0.0
ROW	741	742	743
VALUE	0.0	0.0	0.0
ROW	751	752	753
VALUE	0.0	0.0	0.0
ROW	761	762	763
VALUE	0.0	0.0	0.0
ROW	771	772	773
VALUE	0.0	0.0	0.0
ROW	781	782	783
VALUE	0.0	0.0	0.0
ROW	791	792	793
VALUE	0.0	0.0	0.0
ROW	801	802	803
VALUE	0.0	0.0	0.0
ROW	811	812	813
VALUE	0.0	0.0	0.0
ROW	821	822	823
VALUE	0.0	0.0	0.0
ROW	831	832	833
VALUE	0.0	0.0	0.0
ROW	841	842	843
VALUE	0.0	0.0	0.0
ROW	851	852	853
VALUE	0.0	0.0	0.0
ROW	861	862	863
VALUE	0.0	0.0	0.0
ROW	871	872	873
VALUE	0.0	0.0	0.0
ROW	881	882	883
VALUE	0.0	0.0	0.0
ROW	891	892	893
VALUE	0.0	0.0	0.0
ROW	901	902	903
VALUE	0.0	0.0	0.0
ROW	911	912	913
VALUE	0.0	0.0	0.0
ROW	921	922	923
VALUE	0.0	0.0	0.0
ROW	931	932	933
VALUE	0.0	0.0	0.0
ROW	941	942	943
VALUE	0.0	0.0	0.0
ROW	951	952	953
VALUE	0.0	0.0	0.0
ROW	961	962	963
VALUE	0.0	0.0	0.0
ROW	971	972	973
VALUE	0.0	0.0	0.0
ROW	981	982	983
VALUE	0.0	0.0	0.0
ROW	991	992	993
VALUE	0.0	0.0	0.0
ROW	1001	1002	1003
VALUE	0.0	0.0	0.0

FIG. 15 FORCE AND DISPLACEMENT TABLES FROM STRESS ANALYSIS

STRESS ANALYSIS FOR CASE 1 WING LUG PGM TEST CASE #4A: ALUMINUM LUG FOR STRESSES ONLY

LNUN	CENTROID LOCATION,			CARTESIAN STRESSES			POLAR STRESSES		
	---XC---	---YC---	---ZC---	---XX---	---YY---	---ZZ---	---RR---	---TT---	---RT---

PART A: BUSHING									
1	0.319E+01	0.421E+00	0.421E+00	-0.112E+05	0.156E+04	-0.197E+04	-0.115E+05	0.185E+04	-0.246E+03
2	0.369E+01	0.485E+00	0.485E+00	-0.895E+04	0.213E+04	-0.195E+04	-0.931E+04	0.244E+04	-0.448E+03
3	0.298E+01	0.123E+01	0.123E+01	-0.811E+04	0.685E+03	-0.536E+04	-0.106E+05	0.319E+04	-0.683E+03
4	0.343E+01	0.142E+01	0.142E+01	-0.586E+04	0.708E+03	-0.504E+04	-0.846E+04	0.331E+04	-0.124E+04
5	0.256E+01	0.196E+01	0.196E+01	-0.260E+04	-0.740E+03	-0.723E+04	-0.89CE+04	0.556E+04	-0.974E+03
6	0.295E+01	0.226E+01	0.226E+01	-0.842E+03	-0.120E+04	-0.610E+04	-0.687E+04	0.483E+04	-0.175E+04
7	0.196E+01	0.256E+01	0.256E+01	0.390E+04	-0.198E+04	-0.693E+04	-0.649E+04	0.841E+04	-0.105E+04
8	0.226E+01	0.295E+01	0.295E+01	0.421E+04	-0.228E+04	-0.459E+04	-0.469E+04	0.662E+04	-0.184E+04
9	0.123E+01	0.298E+01	0.298E+01	0.949E+04	-0.212E+04	-0.457E+04	-0.365E+04	0.110E+05	-0.875E+03
10	0.142E+01	0.343E+01	0.343E+01	0.770E+04	-0.163E+04	-0.262E+04	-0.212E+04	0.818E+04	-0.145E+04
11	0.421E+00	0.319E+01	0.319E+01	0.125E+05	-0.267E+03	-0.120E+04	-0.360E+03	0.126E+05	-0.495E+03
12	0.485E+00	0.369E+01	0.369E+01	0.884E+04	0.425E+03	-0.685E+03	0.391E+03	0.887E+04	-0.427E+03
13	-0.421E+00	0.319E+01	0.319E+01	0.120E+05	0.111E+04	0.643E+03	0.113E+04	0.120E+05	0.790E+03
14	-0.485E+00	0.369E+01	0.369E+01	0.857E+04	0.143E+04	-0.253E+03	0.162E+04	0.839E+04	0.117E+04
15	-0.123E+01	0.298E+01	0.298E+01	0.878E+04	0.116E+04	0.218E+04	0.732E+03	0.920E+04	0.115E+04
16	-0.142E+01	0.343E+01	0.343E+01	0.750E+04	0.743E+03	0.329E+03	0.150E+04	0.674E+04	0.216E+04
17	-0.196E+01	0.256E+01	0.256E+01	0.488E+04	0.113E+04	0.211E+04	0.487E+03	0.553E+04	0.126E+04
18	-0.226E+01	0.295E+01	0.295E+01	0.544E+04	-0.733E+02	0.926E+03	0.107E+04	0.429E+04	0.242E+04
19	-0.256E+01	0.196E+01	0.196E+01	0.190E+04	0.150E+03	0.110E+04	0.195E+03	0.186E+04	0.113E+04
20	-0.295E+01	0.226E+01	0.226E+01	0.315E+04	-0.727E+03	0.113E+04	0.617E+03	0.180E+04	0.217E+04
21	-0.298E+01	0.123E+01	0.123E+01	0.378E+03	-0.150E+04	0.188E+03	-0.302E+02	-0.109E+04	0.796E+03
22	-0.343E+01	0.142E+01	0.142E+01	0.127E+04	-0.116E+04	0.932E+03	0.254E+03	-0.150E+03	0.152E+04
23	-0.319E+01	0.421E+00	0.421E+00	-0.124E+03	-0.278E+04	-0.594E+02	-0.153E+03	-0.275E+04	0.286E+03
24	-0.369E+01	0.485E+00	0.485E+00	0.189E+03	-0.135E+04	0.355E+03	0.701E+02	-0.127E+04	0.548E+03
25	-0.319E+01	-0.421E+00	-0.421E+00	-0.124E+03	-0.278E+04	0.598E+02	-0.153E+03	-0.275E+04	-0.285E+03
26	-0.369E+01	-0.485E+00	-0.485E+00	0.189E+03	-0.139E+04	-0.354E+03	0.701E+02	-0.127E+04	-0.547E+03
27	-0.298E+01	-0.123E+01	-0.123E+01	0.378E+03	-0.150E+04	-0.188E+03	-0.301E+02	-0.109E+04	-0.796E+03
28	-0.343E+01	-0.142E+01	-0.142E+01	0.127E+04	-0.117E+04	-0.931E+03	0.254E+03	-0.150E+03	-0.152E+04
29	-0.256E+01	-0.196E+01	-0.196E+01	0.190E+04	0.148E+03	-0.110E+04	0.194E+03	0.186E+04	-0.113E+04
30	-0.295E+01	-0.226E+01	-0.226E+01	0.315E+04	-0.727E+03	-0.113E+04	0.616E+03	0.180E+04	-0.217E+04
31	-0.196E+01	-0.421E+00	-0.421E+00	0.488E+04	0.111E+04	-0.211E+04	0.211E+04	0.553E+04	0.553E+04

FIG. 16 PART OF STRESS TABLE

STRESS INTENSITIES POP CASE 36 LUG PROGRAM STRESS INTENSITY ANALYSIS

POS	---ANGLES---	---K1---	---K2---
1	0.0	0.382E+03	0.869E-01
2	0.112E+02	0.421E+03	0.207E+02
3	0.225E+02	0.488E+03	0.509E+01
4	0.337E+02	0.506E+03	0.370E+02
5	0.450E+02	0.489E+03	0.172E+02
6	0.562E+02	0.495E+03	0.390E+02
7	0.675E+02	0.532E+03	0.720E+02
8	0.787E+02	0.594E+03	0.579E+02
9	0.900E+02	0.713E+03	0.679E+01
10	0.101E+03	0.876E+03	0.233E+03
11	0.112E+03	0.927E+03	0.409E+03
12	0.124E+03	0.773E+03	0.403E+03
13	0.135E+03	0.528E+03	0.267E+03
14	0.146E+03	0.298E+03	0.152E+03
15	0.157E+03	0.106E+03	0.998E+02
16	0.169E+03	-0.313E+02	0.582E+02
17	0.180E+03	-0.813E+02	0.208E-01
18	0.191E+03	-0.312E+02	0.582E+02
19	0.202E+03	0.106E+03	0.998E+02
20	0.214E+03	0.298E+03	0.151E+03
21	0.225E+03	0.528E+03	0.267E+03
22	0.236E+03	0.773E+03	0.403E+03
23	0.247E+03	0.927E+03	0.409E+03
24	0.259E+03	0.876E+03	0.233E+03
25	0.270E+03	0.714E+03	0.675E+01
26	0.281E+03	0.595E+03	0.580E+02
27	0.292E+03	0.533E+03	0.723E+02
28	0.304E+03	0.496E+03	0.393E+02
29	0.315E+03	0.490E+03	0.168E+02
30	0.326E+03	0.506E+03	0.366E+02
31	0.337E+03	0.487E+03	0.529E+01
32	0.349E+03	0.421E+03	0.205E+02

FIG. 17 STRESS INTENSITY FACTOR TABLE FROM ANALYSIS WITH NT = 4

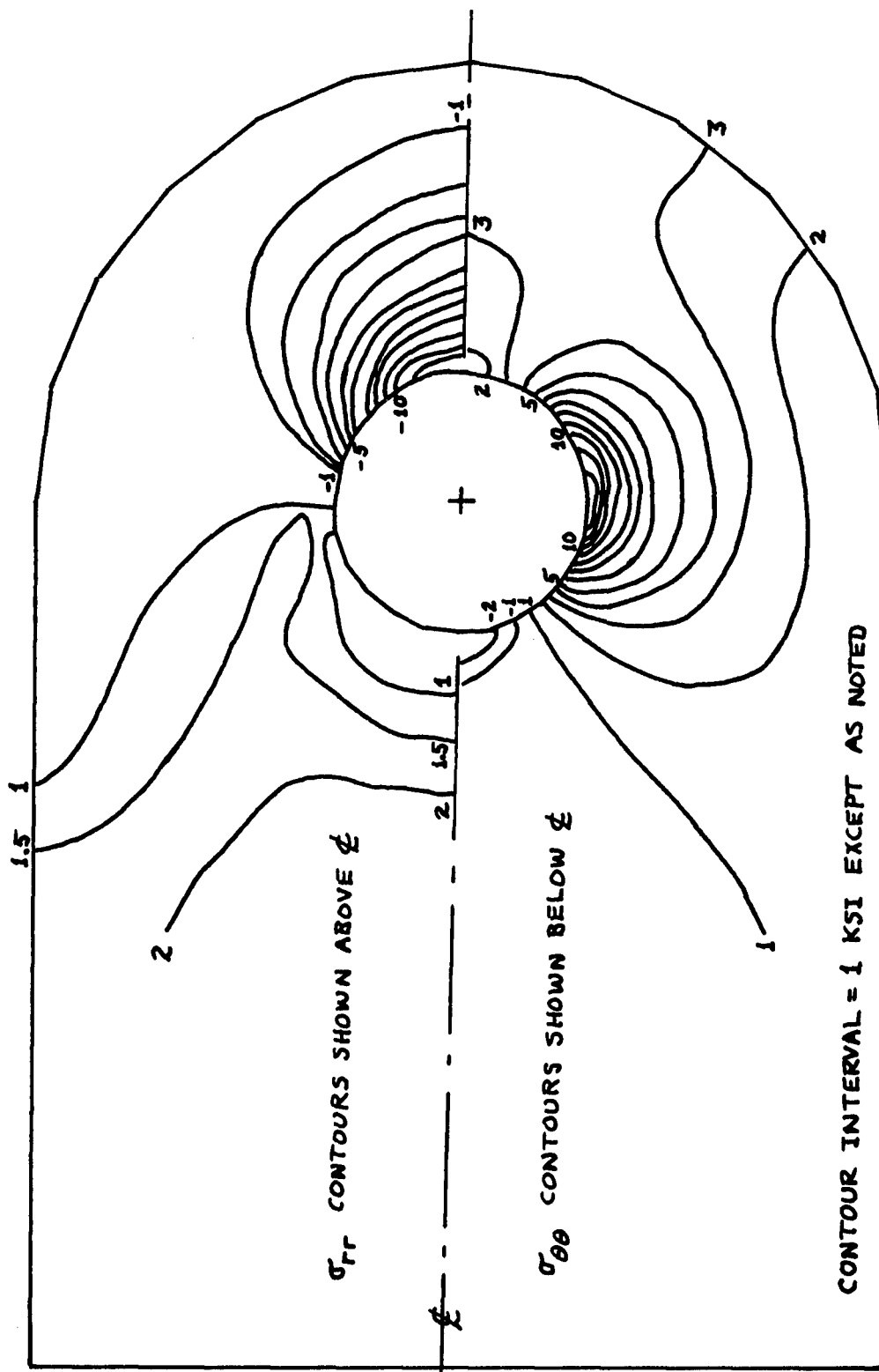


FIG. 18 STRESS CONTOURS FOR WING ROOT LUG

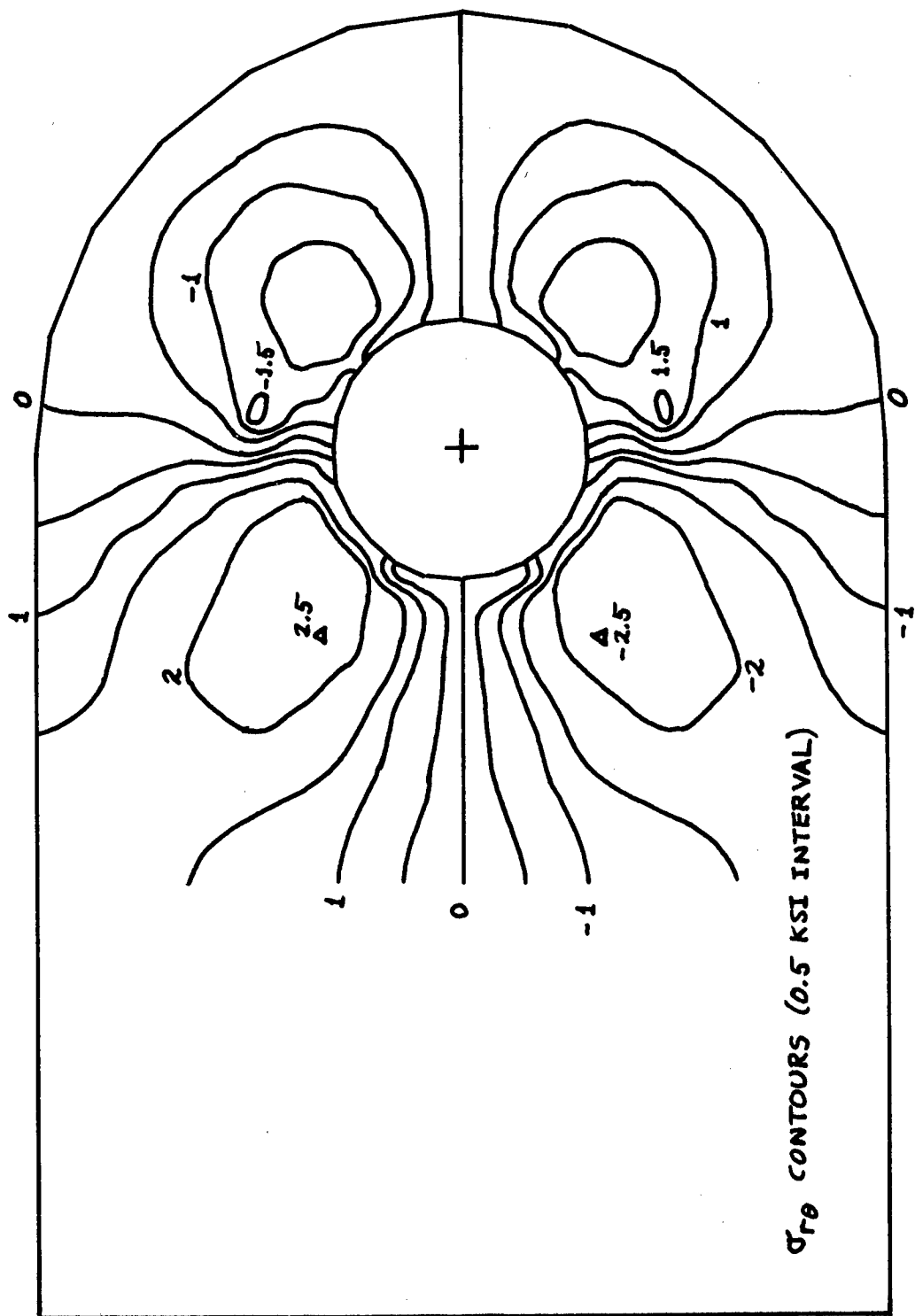


FIG. 18 (CONCLUDED)

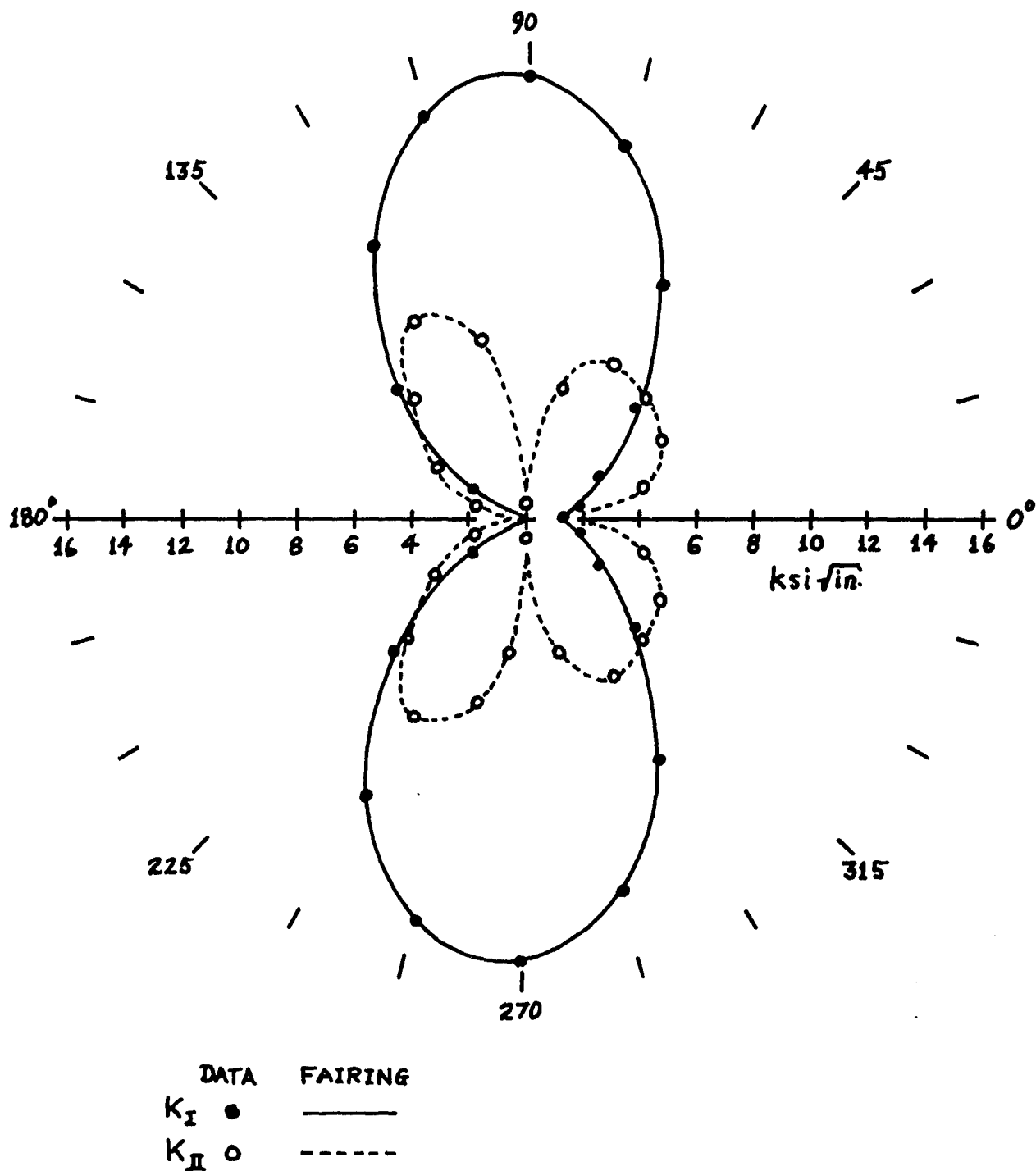


FIG. 19 BUTTERFLY PLOT FOR WING ROOT LUG STRESS INTENSITIES

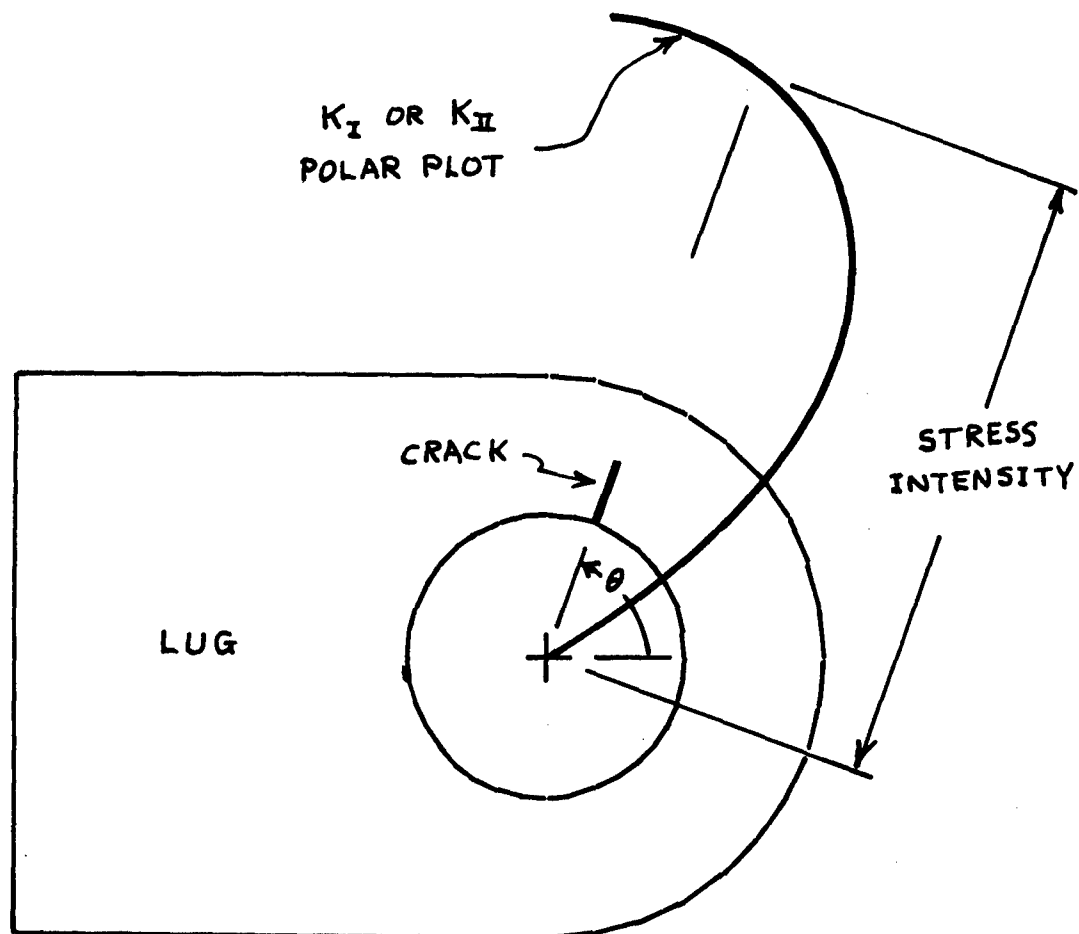


FIG. 20 INTERPRETATION OF BUTTERFLY PLOTS

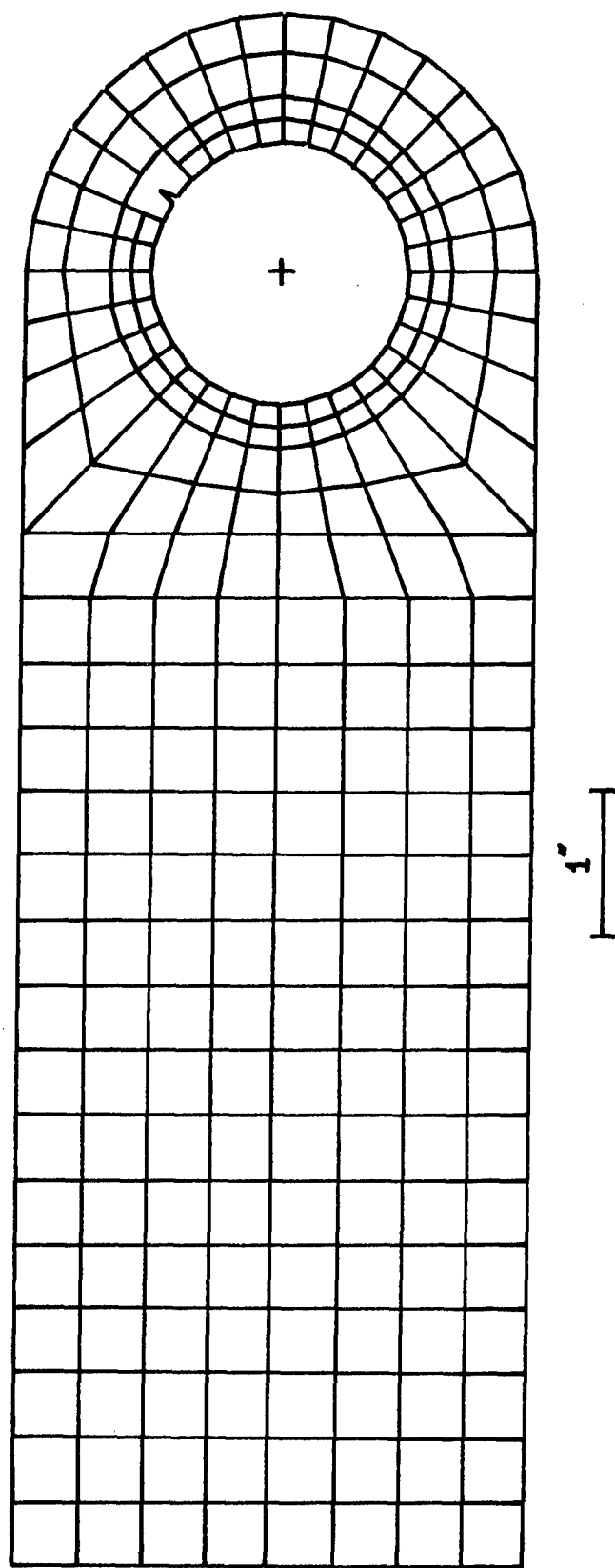


FIG. 21 SCALE MESH PLAN FOR ENGINE PYLON TRUSS LUG

Figure 1 consists of two contour plots arranged vertically, showing the distribution of stress components in a semi-circular domain. The top plot displays the stress component $\sigma_{\theta\theta}$ with contours labeled 1.5, 1, 0, -1, and -1.5. The bottom plot displays the stress component σ_{rr} with contours labeled 3, 2, 1, 0, -1, -2, -3, and -4. Both plots have a central circular region labeled $\sigma_{rr} + \sigma_{\theta\theta}$.

57

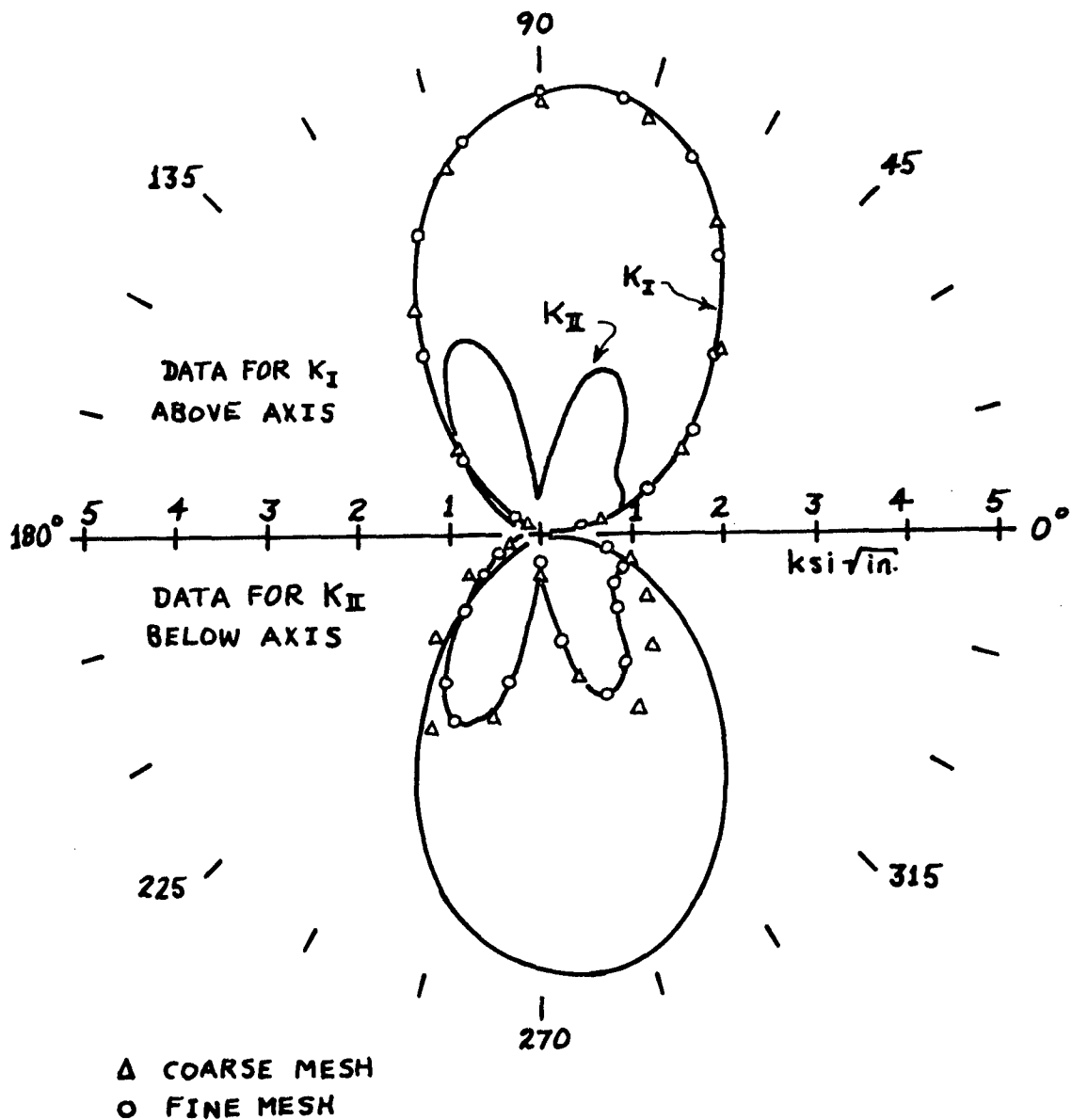
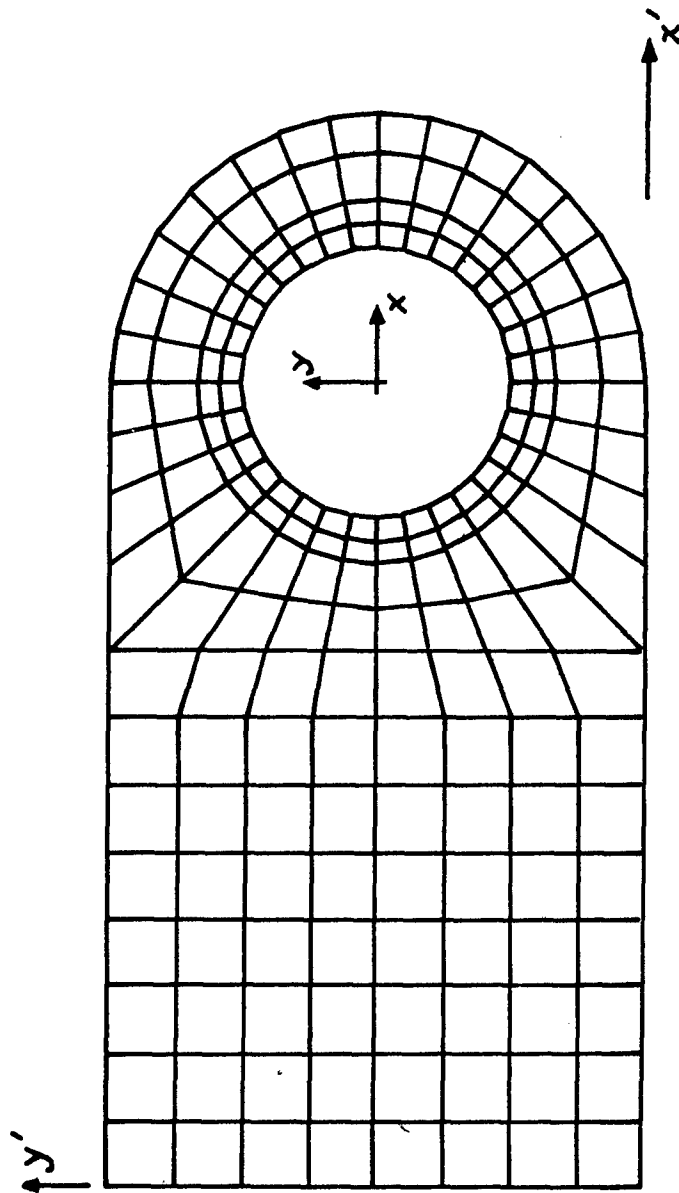


FIG. 23 BUTTERFLY PLOT FOR ENGINE PYLON TRUSS LUG
(TENSION BEARING, COSINE PRESSURE)



Note: $x'y'$ axes refer to comparison of results with engineering beam theory (Fig. 29).

FIG. 24 SCALE MESH PLAN FOR 7-INCH ENGINE PYLON TRUSS LUG

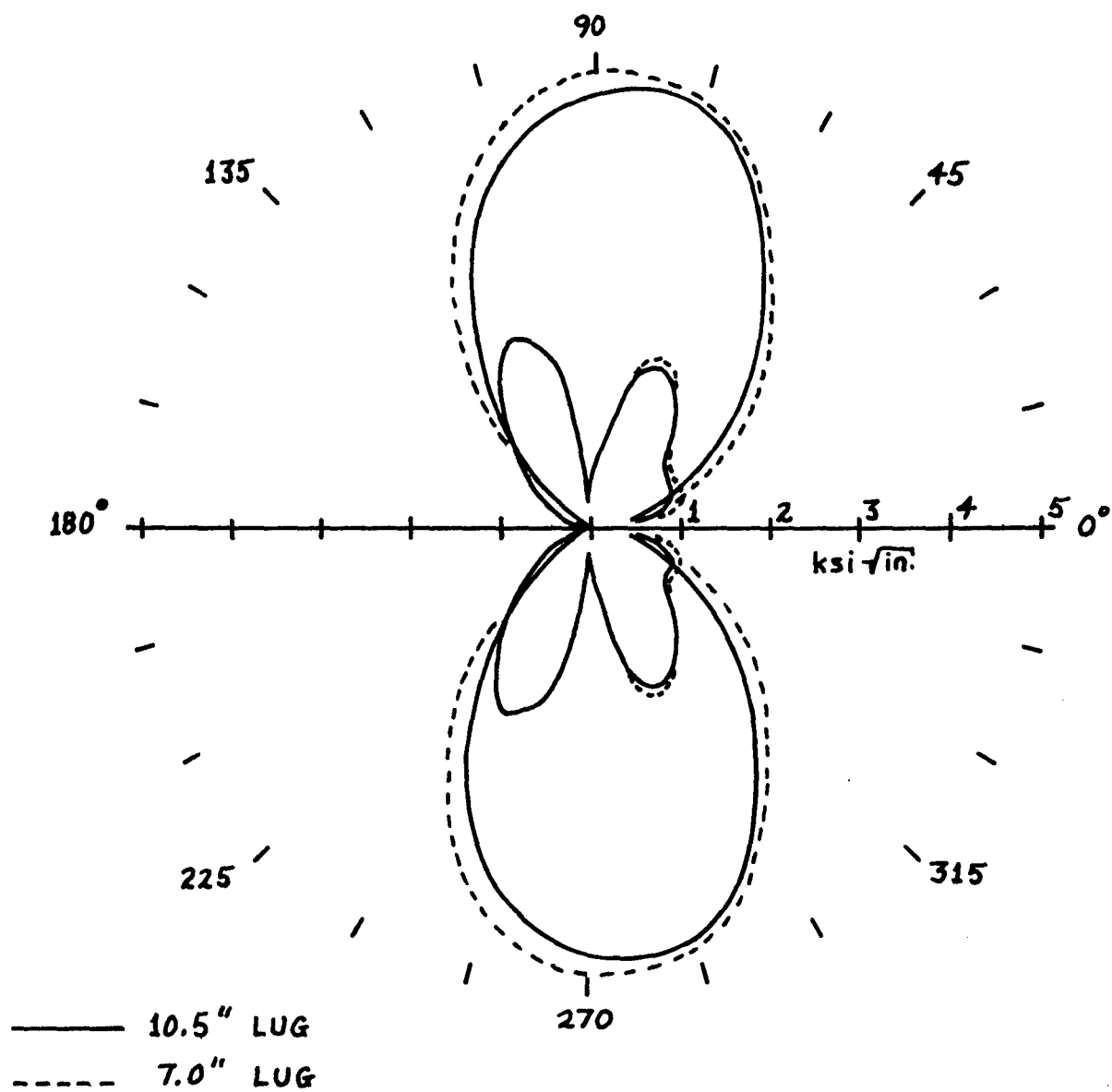


FIG. 25 EFFECT OF SHANK LENGTH ON STRESS INTENSITY
(TENSION BEARING, COSINE PRESSURE)

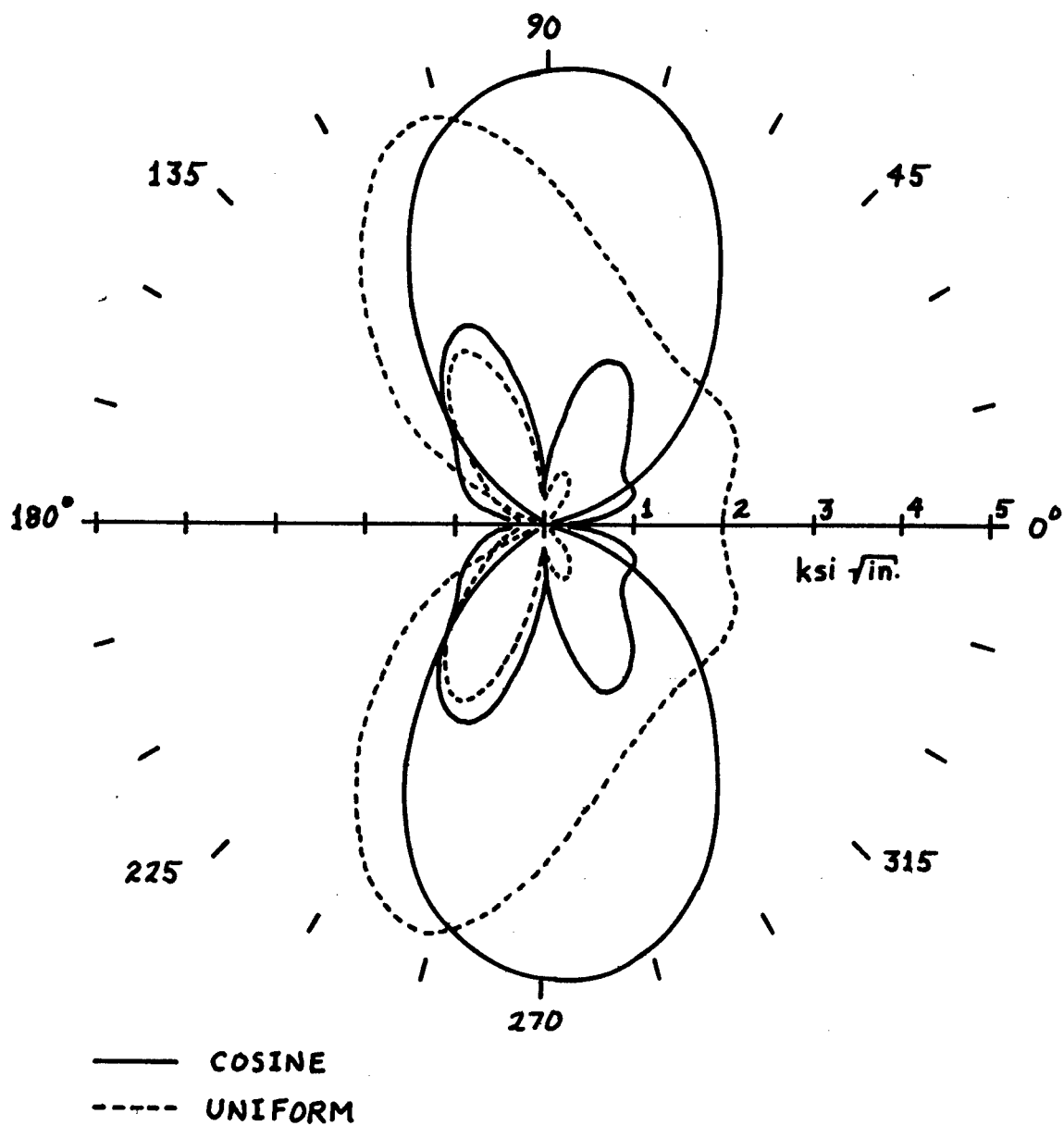


FIG. 26 COMPARISON OF COSINE AND UNIFORM PRESSURE DISTRIBUTIONS (TENSION BEARING)

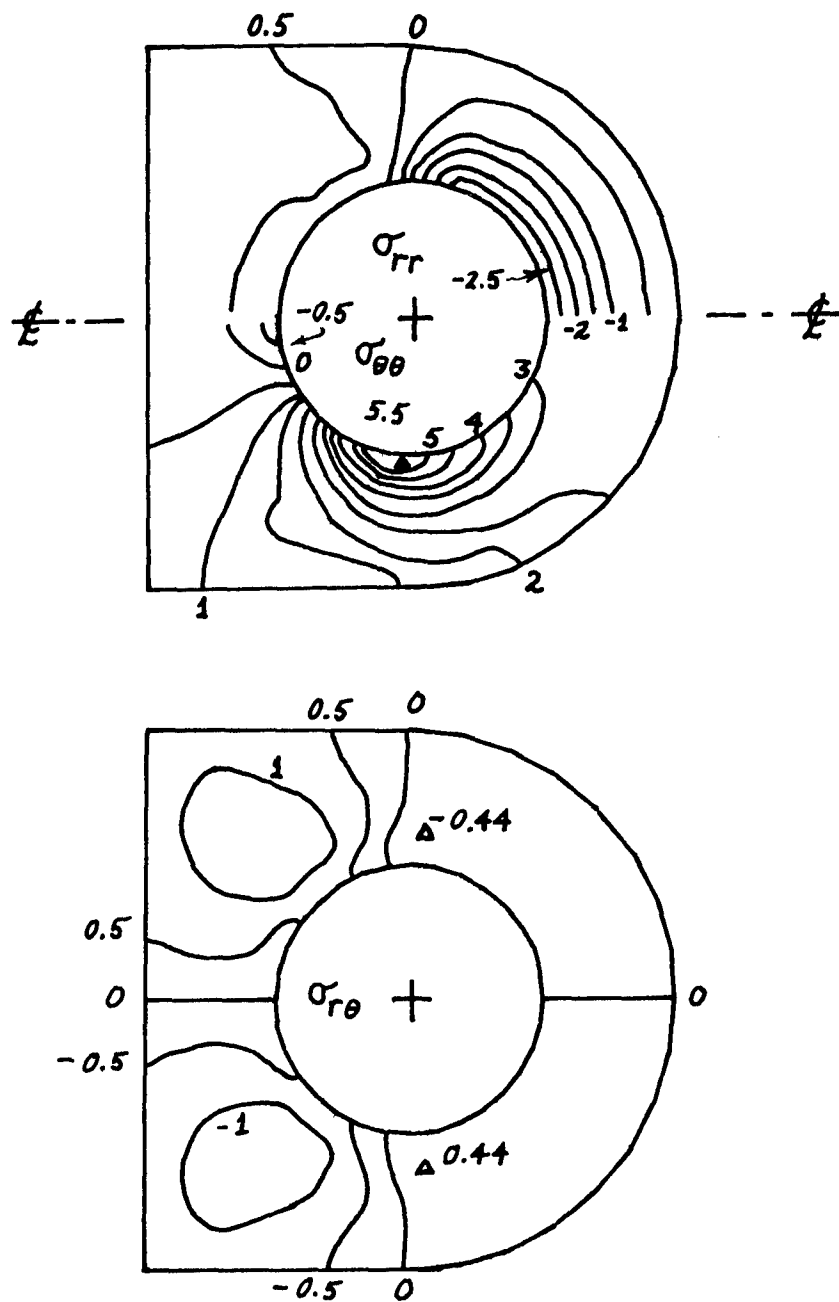


FIG. 27 STRESS CONTOURS FOR 7-INCH ENGINE PYLON TRUSS LUG (TENSION BEARING, UNIFORM PRESSURE)

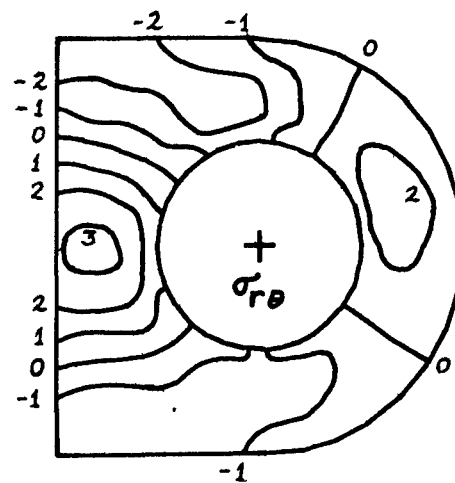
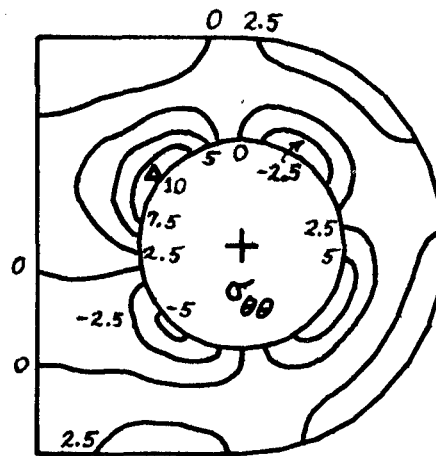
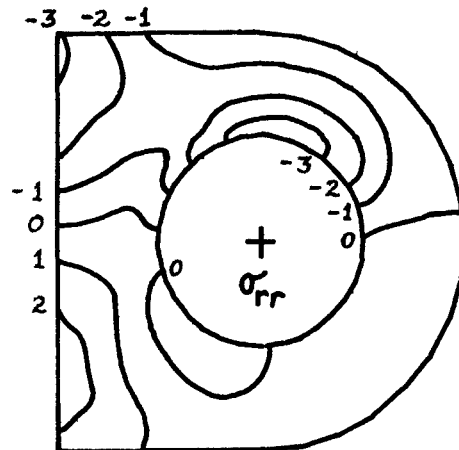
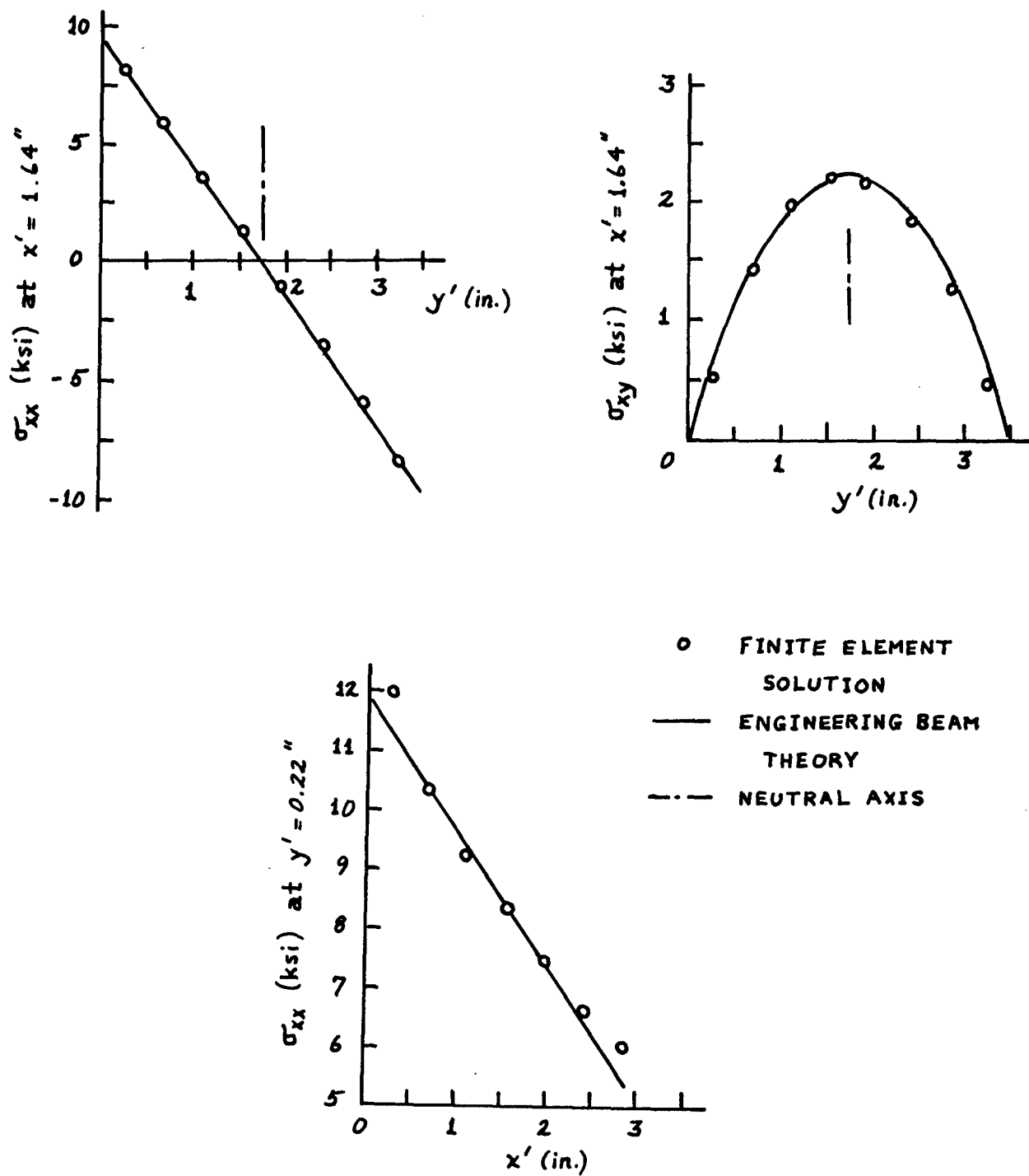


FIG. 28 STRESS CONTOURS FOR 7-INCH ENGINE PYLON TRUSS LUG (POSITIVE SHEAR BEARING, COSINE PRESSURE)



Note: See Fig. 24 for location of $x'y'$ axes

FIG. 29 COMPARISON OF FINITE ELEMENT RESULTS WITH ENGINEERING BEAM THEORY (POSITIVE SHEAR BEARING, COSINE PRESSURE)

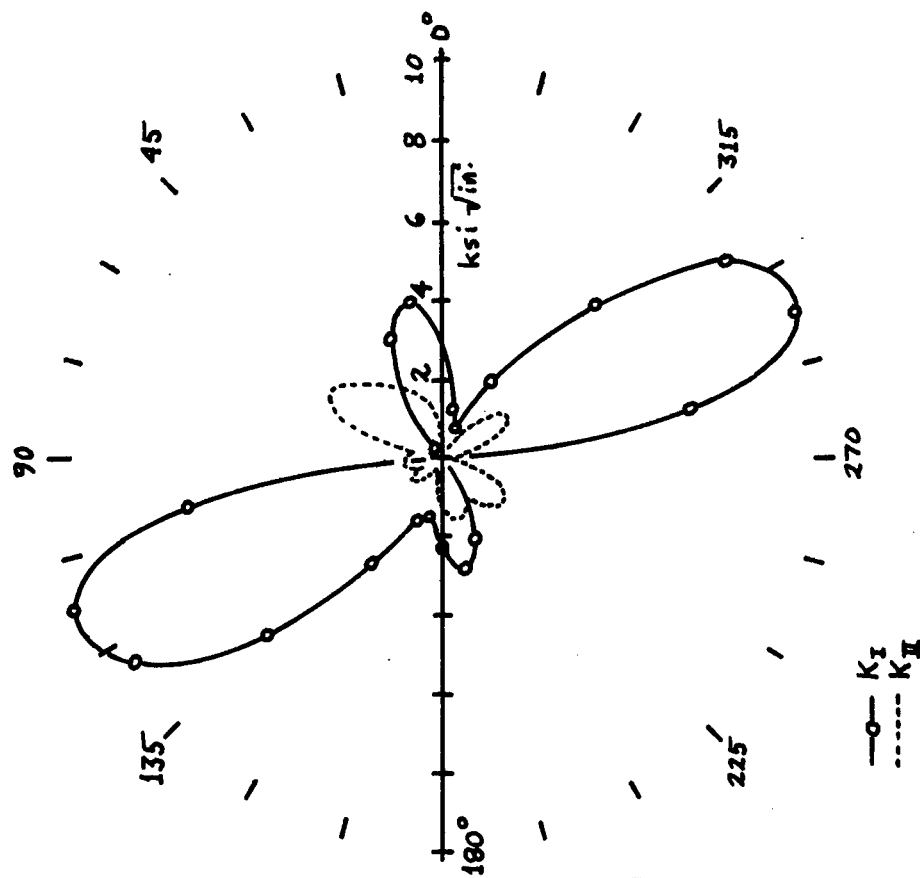


FIG. 30 BUTTERFLY PLOTS FOR 7-INCH ENGINE PYLON TRUSS LUG (POSITIVE SHEAR BEARING, COSINE PRESSURE)

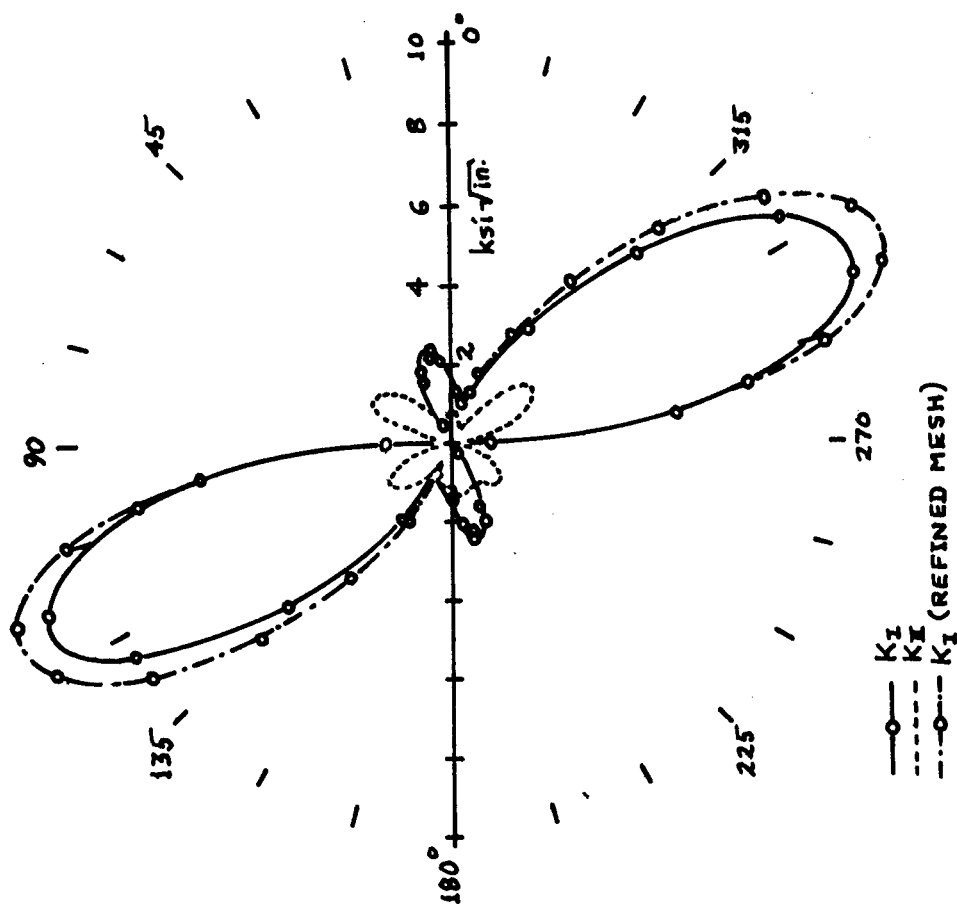


FIG. 31 BUTTERFLY PLOTS FOR 7-INCH PYLON TRUSS LUG (POSITIVE SHEAR BEARING, UNIFORM PRESSURE)

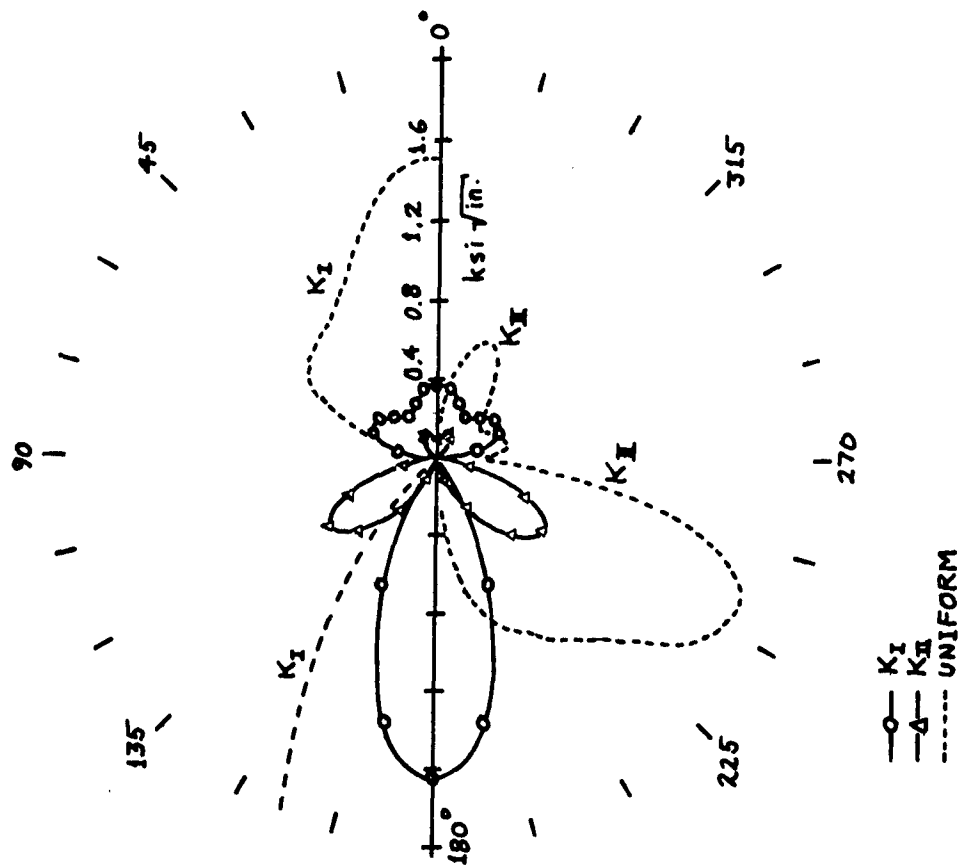


FIG. 32 BUTTERFLY PLOTS FOR 7-INCH ENGINE
PYLON TRUSS LUG (COMPRESSION
BEARING, COSINE PRESSURE)

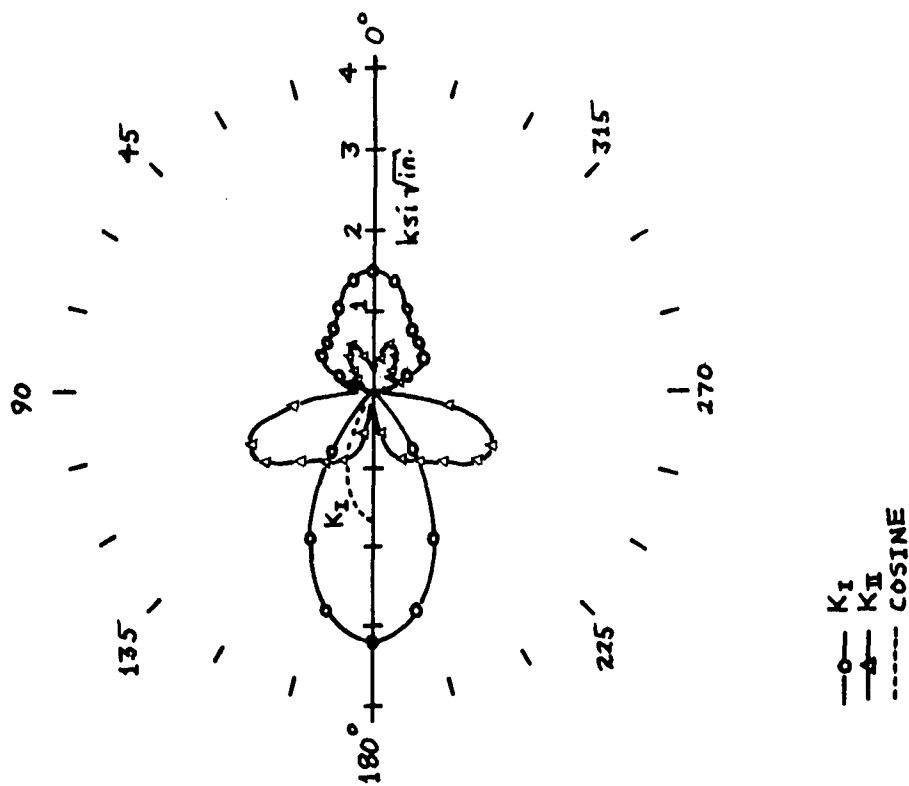


FIG. 33 BUTTERFLY PLOTS FOR 7-INCH
ENGINE PYLON TRUSS LUG
(COMPRESSION BEARING, UNIFORM
PRESSURE)

APPENDIX A

```

*****
C
C ATTACHMENT LUG PROCEDURE (LUG)
C
C PROCEDURE LUG IS A FINITE-ELEMENT ANALYSIS PROGRAM FOR STRESS ANALYSIS AND/OR
C CALCULATION OF NASA/ASTM STANDARD STRESS INTENSITY FACTORS IN A ONE- OR TWO-
C MATERIAL LUG SUBJECTED TO A BEARING LOAD.
C
C PROCEDURE LUG AUTOMATICALLY GENERATES A STRUCTURE MODEL REPRESENTING AN ATTACHMENT LUG
C PARALLEL TO THE X-AXIS. THE LEFT (VERTICAL) EDGE OF THE LUG IS BUILT IN.
C THE LUG BEGINS WITH CONSTANT WIDTH (Y-DIRECTION) AND FAIRS INTO A SEMI-
C CIRCULAR SHAPE ON THE RIGHT. AN INTEGRALLY BONDED ISOTROPIC BUSHING (MATL
C #1) IS CONCENTRIC WITH THE SEMI-CIRCLE. THE LUG (MATL #2) MAY BE ISOTROPIC
C OR ORTHOTROPIC WITH MATERIAL AXES INCLINED AT AN ARBITRARY ANGLE TO THE XY
C AXIS SYSTEM. A COSINE OR UNIFORM PRESSURE BEARING LOAD IS APPLIED TO THE
C INNER SURFACE OF THE BUSHING, CENTERED ON THE LINE OF ACTION OF THE
C RESULTANT BEARING FORCE. THE BEARING FORCE IS INPUT AS A TENSION COMPONENT
C (PARALLEL TO X, POSITIVE TO RIGHT) AND A SHEAR COMPONENT (PARALLEL TO Y,
C POSITIVE UP). PLANE STRESS IS ASSUMED. MULTIPLE CASES MAY BE RUN BY
C REPEATING CARDS 2 THRU 7 OF THE INPUT DATA CARD STACK.
C
C INPUT DATA CARD STACK:
C 1. NCASES
C 2. TITLE
C 3. IANL, LOAD, MCDE, NT
C 4. DI, DB, W, H, T, CSIZE
C 5. E1, V1
C 6. E2, V2
C OR
C EL2, ELT2, FT2, G2, THETA
C 7. TENSIN, SHEAR
C
C EXPLANATION:
C NCASES = TOTAL NO. OF CASES TO BE RUN
C TITLE = ANY DESCRIPTIVE INFORMATION FOR THIS CASE
C IANL = ANALYSIS OPTION: 1 = STRESS ANALYSIS AND FULL PRINT
*****

```



```

EQUIVALENCE (E(1,1), C(1,1))
C STORAGE FOR STRESS INTENSITY RESULTS
  DIMENSION ONE(48), TWO(48), ANGLE(48)
  DATA TEMP/4*0./, NOD/4*0./, CB/9*0./, PI/3.141593/
C READ/PRINT CONTROL
500 FORMAT(16I5)
501 FORMAT(8E10.3)
502 FORMAT(20A4)
600 FORMAT(4(1X,30(4H****)),/,36H0FEABL-2 WING ATTACH LUG PROGRAM FOLUG 0021
2R,I4,6H CASES,/,4(1X,30(4H****)),/)
601 FORMAT(5H1CASE,I4,1H:,1X,20A4)
602 FORMAT(6HCMODE=,I2,33H (1=ISOTROPIC, 2=ORTHOTROPIC LUG),/,1X,8HTOTLUG 0024
2AL OF,I3,25H ELEMENTS AROUND PIN HOLE,/,1X,10H HOLE I.D.=,E10.3,5X,LUG 0025
313HBUSHING O.D.=,E10.3,5X,10H LUG WIDTH=,E10.3,2X,11H LUG LENGTH=, LUG 0026
4 E10.3,2X,10H THICKNESS=,E10.3)
603 FORMAT(21H0BUSHING MATERIAL: E=,E10.3,4H NU=,E10.3)
6041 FORMAT(21H0ISOTROPIC LUG: E=,E10.3,4H NU=,E10.3)
6042 FORMAT(4H0ORTHOTROPIC LUG WITH MATERIAL AXES INCLINED,E10.3,18H DLUG 0030
2EG AND C MATRIX=,3X,3E15.3,/,2(75X,3E15.3,/))
605 FORMAT(17H0APPLIED TENSION=,E10.3,15H LB. AND SHEAR=,E10.3,4H LB.) LUG 0032
606 FORMAT(1HC,10(4H****)),/,39H0INDEFINITE MATRIX; THIS CASE CANCELLED LUG 0033
2,/,1X,10(4H****))
607 FORMAT(25H1STRESS ANALYSIS FOR CASE,I4,1X,20A4,/,5H0LNUM,4X,18HCENLUG 0035
2TFOLD LOCATION,12X,18HCARTESIAN STRESSES,20X,14HPOLAR STRESSES,/, LUG 0036
3 7X,10H-----XC-----,2X,10H-----YC-----,2X,10H-----XX-----,2X,10H-----YY-----LUG 0037
4--,2X,10H-----XY-----,2X,10H-----RR-----,2X,10H-----TT-----,2X,10H-----RTLUG 0038
5-----,/,1X,25(4H****)),/,1X,15HPART A: BUSHING)
608 FORMAT(1X,11HPART B: LUG)
609 FORMAT(1X,I4,8(2X,E10.3))
610 FORMAT(28H1STRESS INTENSITIES FOR CASE,I4,1X,20A4,/,4H POS,7X,10H LUG 0042
2---ANGLES---,2X,10H-----K1-----,2X,10H-----K2-----,/,1X,46(1H*))
611 FORMAT(1X,I3,7X,E10.3,2X,E10.3,2X,E10.3)
612 FORMAT(17H0ANALYSIS OPTION=,I2,14H; LCAL OPTION=,I2)
613 FORMAT(14H0CRACK LENGTH=,E10.3,12H; DIRECTION=,E10.3)
SQPI = SQRT(PI)
C DEVICE CODES

```

```

KR = 5
KW = 6
READ (KR,500) NCASES
WRITE (KW,600) NCASES
C CASE LOOP
DO 32 ICASE = 1, NCASES
  KT1 = KW
  READ (KR,502) TITLE
  WRITE (KW,601) ICASE, TITLE
  READ (KR,500) IANL,LOAD,MODE,NT
  C IANL = 1 (STRESS ANALYSIS; NO CRACK) OR 2 (STRESS INTENSITY ANALYSIS
  C WITH CRACK SEQUENCED AROUND PIN HCLE)
  C LOAD = 1 (COSINE BEARING) OR 2 (CONSTANT BEARING) OVER 180-DEG ARC
  C MODE = 1 (ISOTROPIC LUG) OR 2 (ORTHOTROPIC LUG)
  C NT = DIVISIONS PER 45 DEG AROUND PIN HCLE
    NT2 = 2*NT
    NT2P1 = NT2+1
    NT3P1 = 3*NT+1
    NT4P1 = 4*NT+1
    NT5P1 = 5*NT+1
    NT6P1 = 6*NT+1
    NT8 = 8*NT
    MAXLOC = 1
    IF (IANL .EQ. 2) MAXLOC = NT8
    AINC = 0.25*PI/NT
    READ (KR,501) DI, DB, W, H, T, CSIZE, CDIR
    AAA2 = 0.
    AAA3 = -PI/2.
    AAA4 = AINC/2.
    TWOPI = 2./PI
    DO 100 I = 3, NT8, 2
      AAA2 = AAA2+AINC
      AAA3 = AAA3+AINC
      AAA1 = TWOPI*(SIN(AAA3+AAA4) - SIN(AAA3-AAA4))
      IP1 = I+1
      CA2 = COS(AAA2)

```

```

LUG 0049
LUG 0050
LUG 0051
LUG 0052
LUG 0053
LUG 0054
LUG 0055
LUG 0056
LUG 0057
LUG 0058
LUG 0059
LUG 0060
LUG 0061
LUG 0062
LUG 0063
LUG 0064
LUG 0065
LUG 0066
LUG 0067
LUG 0068
LUG 0069
LUG 0070
LUG 0071
LUG 0072
LUG 0073
LUG 0074
LUG 0075
LUG 0076
LUG 0077
LUG 0078
LUG 0079
LUG 0080
LUG 0081
LUG 0082
LUG 0083
LUG 0084

```

```

SA2 = SIN(AAA2)
SCALE(I,1) = AAA1*CA2
SCALE(IP1,1) = AAA1*SA2
SCALE(I,2) = AAA4*CA2
100 SCALE(IP1,2) = AAA4*SA2
SCALE(1,1) = 0.
SCALE(1,2) = 0.5*AAA4
SCALE(2,1) = 0.
SCALE(2,2) = 0.
SCALE(NT8+1,1) = 0.
SCALE(NT8+2,1) = 0.
SCALE(NT8+1,2) = -0.5*AAA4
SCALE(NT8+2,2) = 0.
C DI = PIN HOLE DIAMETER
C DE = BUSHING O.D.
C W = LUG WIDTH
C H = LUG LENGTH
C T = PART THICKNESS
C CSIZE = CRACK SIZE
C CDIR = CCW ANGLE FROM BEARING SURFACE OUTWARD NORMAL TO LINE OF
C      CRACK (DEGREE MEASURE)
      WRITE (KW,612) IANL, LOAD
      WRITE (KW,602) MCDE, NT8, DI, DB, W, H, T
      IF (IANL.EQ. 2) WRITE (KW,613) CSIZE, CDIR
      RI = 0.5*DI
      RB = 0.5*DB
      RL = 0.5*W
      A = H-W
C BUSHING MATERIAL (ALWAYS ISOTROPIC)
      READ (KR,501) E, V
      WRITE (KW,603) E, V
      CB(1,1) = E/(1.-V*V)
      CB(2,1) = V*CB(1,1)
      CB(1,2) = CB(2,1)
      CB(2,2) = CB(1,1)
      CB(3,3) = 0.5*E/(1.+V)
LUG 0085
LUG 0086
LUG 0087
LUG 0088
LUG 0089
LUG 0090
LUG 0091
LUG 0092
LUG 0093
LUG 0094
LUG 0095
LUG 0096
LUG 0097
LUG 0098
LUG 0099
LUG 0100
LUG 0101
LUG 0102
LUG 0103
LUG 0104
LUG 0105
LUG 0106
LUG 0107
LUG 0108
LUG 0109
LUG 0110
LUG 0111
LUG 0112
LUG 0113
LUG 0114
LUG 0115
LUG 0116
LUG 0117
LUG 0118
LUG 0119
LUG 0120

```



```

      G = CB(3,3)
      ETA = (3.-V)/(1.+V)
C LUG MATERIAL
      GO TO (1,2), MCDE
C ISOTROPIC
      1 READ (KR,501) E, V
      WRITE (KW,6041) E, V
      CL(1,1) = E/(1.-V*V)
      CL(1,2) = V*CL(1,1)
      CL(2,2) = CL(1,1)
      CL(3,3) = 0.5*E/(1.+V)
      GO TO 3
C ORTHOTROPIC
      2 READ (KR,501) CL(1,1), CL(1,2), CL(2,2), CL(3,3), THETA
      C THETA = MATERIAL AXIS INCLINATION (DEGREES)
      3 CL(2,1) = CL(1,2)
      CL(1,3) = 0.
      CL(2,3) = 0.
      CL(3,1) = 0.
      CL(3,2) = 0.
      GO TO (6,4), MODE
      4 WRITE (KW,6042) THETA, CL
      IF (THETA.EQ. 0.) GO TO 6
C SPECIAL TRANSFORMATION FOR CL
      DO 5 I = 1,3
      DO 5 J = 1,3
      5 C(I,J) = CL(I,J)
      THETA = -THETA
      CALL CTFORM(THETA,C,CL)
C APPLIED LOADS
      6 READ (KR,501) TENSX, SHEAR
      WRITE (KW,605) TENSX, SHEAR
      IF (IANL.EQ. 1) GO TO 4000
      TENSX = TENSX/T
      SHEAR = SHEAR/T
      T = 1.0

```

```

LUG 0121
LUG 0122
LUG 0123
LUG 0124
LUG 0125
LUG 0126
LUG 0127
LUG 0128
LUG 0129
LUG 0130
LUG 0131
LUG 0132
LUG 0133
LUG 0134
LUG 0135
LUG 0136
LUG 0137
LUG 0138
LUG 0139
LUG 0140
LUG 0141
LUG 0142
LUG 0143
LUG 0144
LUG 0145
LUG 0146
LUG 0147
LUG 0148
LUG 0149
LUG 0150
LUG 0151
LUG 0152
LUG 0153
LUG 0154
LUG 0155
LUG 0156

```

```

4000 CONTINUE
C TOPOLOGY PARAMETERS AND HOUSEKEEPING; BEGIN BY SIZING THE MESH TO
C KEEP ELEMENT ASPECT RATIOS CLOSE TO UNITY
  E = PI*(RI+RB)/NT8
  NRB = (RB-RI)/E+0.5
  E = PI*(RB+RL)/NT8
  NRL = (RL-RB)/E+0.5
  E = 0.5*W/NT
  NA = A/E+0.5
  IF (NRB .LE. 1) NRB = 2
  IF (NRL .LE. 0) NRL = 1
  IF (NA .LE. 0) NA = 1
  NRBP1 = NRB+1
  NREP2 = NRB+2
  NR = NRB+NRL
  NNR = NR+1
  NDR = 2*NNR
  NETB = NT8*NRB
  NETBP1 = NETB+1
  NM1 = NT8*NR+2*NT*NA
  NET = NM1
  IF (IANL .EQ. 2) NET = NM1+1
  NDT = 2*(NT8*NNR+NA*NT2P1)
  NDW = 4*NT+2
  LIST = 9*NM1
  IF (IANL .EQ. 2) LIST = LIST+19
  IF (IANL .EQ. 1) GO TO 2002
  DC 2001 LOC = 1,MAXLOC
  ONE(LOC) = 0.
  2001 TWC(LOC) = 0.
  C CRACK LOCATION LOOP
  2002 DO 2011 LOC = 1,MAXLOC
    CALL SETUP(LDATA,NDW,LIST,RE,IN)
  C ELEMENT CONNECTIONS (THREE STAGES)
  C STAGE 1: BUSHING
    LP = IMASR

```

```

LUG 0157
LUG 0158
LUG 0159
LUG 0160
LUG 0161
LUG 0162
LUG 0163
LUG 0164
LUG 0165
LUG 0166
LUG 0167
LUG 0168
LUG 0169
LUG 0170
LUG 0171
LUG 0172
LUG 0173
LUG 0174
LUG 0175
LUG 0176
LUG 0177
LUG 0178
LUG 0179
LUG 0180
LUG 0181
LUG 0182
LUG 0183
LUG 0184
LUG 0185
LUG 0186
LUG 0187
LUG 0188
LUG 0189
LUG 0190
LUG 0191
LUG 0192

```

LUG 0193
LUG 0194
LUG 0195
LUG 0196
LUG 0197
LUG 0198
LUG 0199
LUG 0200
LUG 0201
LUG 0202
LUG 0203
LUG 0204
LUG 0205
LUG 0206
LUG 0207
LUG 0208
LUG 0209
LUG 0210
LUG 0211
LUG 0212
LUG 0213
LUG 0214
LUG 0215
LUG 0216
LUG 0217
LUG 0218
LUG 0219
LUG 0220
LUG 0221
LUG 0222
LUG 0223
LUG 0224
LUG 0225
LUG 0226
LUG 0227
LUG 0228

```

L = INASTR+NET
DO 8 J = 1,NT8
DO 8 I = 1,NRB
IN(LP) = L
K = NDR*(J-1)+2*I-1
M = K+NDR
IF (J.EQ. NT8) M = 2*I-1
DO 7 N = 1,4
7 IN(L+N-1) = K+N-1
IN(L+4) = M+2
IN(L+5) = M+3
IN(L+6) = M
IN(L+7) = M+1
LP = LP+1
8 L = L+8

C STAGE 2: SURROUNDING LUG AREA
DO 10 J = 1,NT8
DO 10 I = NRBPI,NR
IN(LP) = L
K = NDR*(J-1)+2*I-1
M = K+NDR
IF (J.EQ. NT8) M = 2*I-1
DO 9 N = 1,4
9 IN(L+N-1) = K+N-1
IN(L+4) = M+2
IN(L+5) = M+3
IN(L+6) = M
IN(L+7) = M+1
LP = LP+1
10 L = L+8

C STAGE 3: LUG FOOT (TRACK NUMBERING IN A DATA VECTOR OVERLAY, WHICH
C WILL END WITH CCNSTRAINED DOF #S IN CORRECT BLOCK)
IN(1) = NT8*NDE+1-NDW
DO 11 J = 2,NDW
11 IN(J) = IN(J-1)+1
DO 15 J = 1,NA

```

```

C ADVANCE THE LINE
DO 12 K = 1,NDW
12 IN(K) = IN(K)+NDW
DO 15 I = 1,NT2
IN(LP) = L
K = 2*I-1
DO 13 N = 1,4
13 IN(L+N-1) = IN(K+N-1)
IN(L+4) = IN(L+2)-NDW
IN(L+5) = IN(L+3)-NDW
IN(L+6) = IN(L)-NDW
IN(L+7) = IN(L+1)-NDW
IF (J.GT. 1) GO TO 14
C SPECIAL CASE FOR FIRST LINE OF ELEMENTS IN THE FOOT
K = (3*NT+1)*NDR-1
IN(L+4) = K+NDR
IN(L+5) = K+1+NDR
IN(L+6) = K
IN(L+7) = K+1
14 LP = LP+1
L = L+8
15 CONTINUE
IF (IANL.EQ. 1) GO TO 2005
C CRACK ELEMENT CVERLAY: BEGIN BY DUMMYING FOUR QUAD4 ELEMENTS OVERLAID
C BY THE PCRK59
K = NRB*(LCC-1)
LDUMY(1) = K+1-NRB
LDUMY(2) = K+1
LDUMY(3) = K+2-NRB
LDUMY(4) = K+2
C POINTER AND DCF FOR PCRK59
IN(LP) = L
K = NDR*(LCC-1)+1
IN(L) = K+4
IN(L+1) = K+5
IN(L+2) = K+4+NDR
LUG 0229
LUG 0230
LUG 0231
LUG 0232
LUG 0233
LUG 0234
LUG 0235
LUG 0236
LUG 0237
LUG 0238
LUG 0239
LUG 0240
LUG 0241
LUG 0242
LUG 0243
LUG 0244
LUG 0245
LUG 0246
LUG 0247
LUG 0248
LUG 0249
LUG 0250
LUG 0251
LUG 0252
LUG 0253
LUG 0254
LUG 0255
LUG 0256
LUG 0257
LUG 0258
LUG 0259
LUG 0260
LUG 0261
LUG 0262
LUG 0263
LUG 0264

```

```

IN(L+3) = K+5+NDR
IN(L+4) = K+2+NDR
IN(L+5) = K+3+NDR
IN(L+6) = K+NDR
IN(L+7) = K+1+NDR
IF (LOC.NE. MAXLOC) GO TO 3000
C READJUST TOP EDGE EOF IF THE PCRK59 RECONNECTS WITH THE NUMBERING
C START LINE
IN(L+2) = 5
IN(L+3) = 6
IN(L+4) = 3
IN(L+5) = 4
IN(L+6) = 1
IN(L+7) = 2
3000 CONTINUE
C LAPPED NODE
IN(L+8) = K
IN(L+9) = K+1
LAPX = IQ+K-1
LAPY = IQ+K
C MOVED NODE
IN(L+10) = K+2
IN(L+11) = K+3
MCVX = IQ+K+1
MCVY = IQ+K+2
DO 2003 N = 1,6
2003 IN(L+11+N) = K-1+N-NDR
IF (LOC.NE. 1) GO TO 2005
C SPECIAL CASE WHEN PCRK59 OVERLAYS NUMBERING START LINE
LDUMY(1) = 2*NT8-1
LDUMY(3) = 2*NT8
N = NDR*(NT8-1)+1
DO 2004 N = 1,6
2004 IN(L+11+N) = M-1+N
2005 CONTINUE
CALL ORK(LDATA,RE,IN)

```

```

LUG 0265
LUG 0266
LUG 0267
LUG 0268
LUG 0269
LUG 0270
LUG 0271
LUG 0272
LUG 0273
LUG 0274
LUG 0275
LUG 0276
LUG 0277
LUG 0278
LUG 0279
LUG 0280
LUG 0281
LUG 0282
LUG 0283
LUG 0284
LUG 0285
LUG 0286
LUG 0287
LUG 0288
LUG 0289
LUG 0290
LUG 0291
LUG 0292
LUG 0293
LUG 0294
LUG 0295
LUG 0296
LUG 0297
LUG 0298
LUG 0299
LUG 0300

```

```

C GLOBAL COORDINATE ALGORITHM: OVERLAY IN FORCE/DISPLACEMENT VECTOR FOR LUG 0301
C LATER CONVENIENCE (THREE STAGES SIMILAR TO CCNNECTIONS) LUG 0302
C STAGE 1: BUSHING LUG 0303
      E = (RE-RI)/NRB LUG 0304
      DO 16 J = 1,NI8 LUG 0305
      THETA = (J-1)*AINC LUG 0306
      DO 16 I = 1,NRBP1 LUG 0307
      K = NDR*(J-1)+2*(I-1) LUG 0308
      R = RI+(I-1)*E LUG 0309
      RE(IQ+K) = R*CCS(THETA) LUG 0310
      16 RE(IQ+1+K) = R*SIN(THETA) LUG 0311
C STAGE 2: SURROUNDING LUG, BY QUIER EDGE + INTERPOLATION LUG 0312
      DO 22 J = 1,NI8 LUG 0313
      THETA = (J-1)*AINC LUG 0314
      K = J*NDR-2 LUG 0315
      IF (J.GT. NT2P1.AND. J.LI. NT6P1) GC TO 17 LUG 0316
C FIRST AND FOURTH QUADRANTS (CIRCULAR ARC) LUG 0317
      RE(IQ+K) = RL*CCS(THETA) LUG 0318
      RE(IQ+1+K) = RL*SIN(THETA) LUG 0319
      GO TO 21 LUG 0320
      17 IF (J.GT. NT4P1) GO TO 19 LUG 0321
C SECOND QUADRANT LUG 0322
      IF (J.GT. NT3P1) GO TO 18 LUG 0323
      RE(IQ+K) = -RL*TAN(THETA-0.5*PI) LUG 0324
      RE(IQ+1+K) = RL LUG 0325
      GO TO 21 LUG 0326
      18 RE(IQ+K) = -RL LUG 0327
      RE(IQ+1+K) = RL*TAN(PI-THETA) LUG 0328
      GO TO 21 LUG 0329
C THIRD QUADRANT LUG 0330
      19 IF (J.GT. NT5P1) GO TO 20 LUG 0331
      RE(IQ+K) = -RL LUG 0332
      RE(IQ+1+K) = -RL*TAN(THETA-PI) LUG 0333
      GO TO 21 LUG 0334
      20 RE(IQ+K) = -RL*TAN(1.5*PI-THETA) LUG 0335
      RE(IQ+1+K) = -RL LUG 0336

```

```

C INTERPOLATION
  21 L = NDR*(J-1)+2*NRB
      E = (RE(IQ+K)-RE(IQ+L))/NRL
      V = (RE(IQ+1+K)-RE(IQ+1+L))/NRL
      DO 22 I = NRB2,NR
        L = L+2
        RE(IQ+L) = RE(IQ+L-2)+E
      22 RE(IQ+1+L) = RE(IQ-1+L)+V
C STAGE 3: LUG FOOT
  K = NT8*NDR
  E = A/NA
  V = W/NT2
  DO 23 J = 1,NA
    DO 23 I = 1,NT2P1
      RE(IQ+K) = -(RL+J+E)
      RE(IQ+1+K) = RL-(I-1)*V
    23 K = K+2
      IF (IANL.EQ. 1) GO TO 2006
C CHANGE COORDINATES OF MOVED NCDE TO LAPPED NCDE
      RE(MOVX) = RE(LAPX)
      RE(MOY) = RE(LAPY)
C ANGLE TO CRACK; TIF COORDINATES
      E = (LOC-1)*AINC
      ANGLE(LOC) = 180.*E/PI
      CDIR = PI*CDIR/180.
      XTIP = RE(LAPX)+CSIZE*COS(CDIR+E)
      YTIP = RE(LAPY)+CSIZE*SIN(CDIR+E)
      2006 CONTINUE
C GENERATION/ASSEMBLY
      IF (IANL.EQ. 1) REWIND 20
      DO 24 K = 1,18
        24 Q(K) = 0.
      DO 26 L = 1,NM1
        IF (IANL.EQ. 1) GO TO 2007
C SKIP DUMMY QUAD4 ELEMENTS IN OVERLAY
      IF (L.EQ. LDUMY(1).OR. L.EQ. LDUMY(2).OR. L.EQ. LDUMY(3)

```

LUG 0337
 LUG 0338
 LUG 0339
 LUG 0340
 LUG 0341
 LUG 0342
 LUG 0343
 LUG 0344
 LUG 0345
 LUG 0346
 LUG 0347
 LUG 0348
 LUG 0349
 LUG 0350
 LUG 0351
 LUG 0352
 LUG 0353
 LUG 0354
 LUG 0355
 LUG 0356
 LUG 0357
 LUG 0358
 LUG 0359
 LUG 0360
 LUG 0361
 LUG 0362
 LUG 0363
 LUG 0364
 LUG 0365
 LUG 0366
 LUG 0367
 LUG 0368
 LUG 0369
 LUG 0370
 LUG 0371
 LUG 0372

```

2 .OR. L.EQ. LDUMY(4)) GO TO 26
2007 CONTINUE
CALL XTRACT(L,8,EXY,RE,IN)
C ... THUS RETRIEVING THE PROPER COORDINATES (CLEVER!!)
E = 0.
V = 0.
DO 25 N = 1,4
E = E+0.25*EXY(2*N-1)
25 V = V+0.25*EXY(2*N)
EXY(11) = EXY(8)
EXY(10) = EXY(7)
EXY(8) = EXY(6)
EXY(7) = EXY(5)
EXY(5) = EXY(4)
EXY(4) = EXY(3)
IF (L.LE. NETE) CALL QUAD4(EXY,T,TEMP,CB,0,NOD,ANG,Q,SM,B,L,KW)
IF (L.GT. NETE) CALL QUAD4(EXY,T,TEMP,CL,0,NOD,ANG,Q,SM,B,L,KW)
IF (IANL.EQ. 1) WRITE (20) B, E, V
CALL ASMLTV(L,8,SM,Q,RE,IN)
26 CCNTINUE
IF (IANL.EQ. 1) GO TO 2008
C ASSEMBLE THE PCRK59
CALL XTRACT(NET,18,EXY,RE,IN)
CALL PCRK59(2,G,FTA,XTIP,YTIP,EXY,SM,BCR)
CALL ASMLTV(NET,18,SM,Q,RE,IN)
2008 CONTINUE
C GET RID OF NODAL CCORDINATES
DO 27 K = IQ,IQ
27 RE(K) = 0.
IF (SHEAR.EQ. 0..AND. TENSIN.EQ. 0.) GO TO 288
IF (SHEAR.EQ. 0.) GO TO 282
C APPLY SHEAR
IFLAG = 1
J3 = 0
J4 = 0
AAA1 = SHEAR

```

```

LUG 0373
LUG 0374
LUG 0375
LUG 0376
LUG 0377
LUG 0378
LUG 0379
LUG 0380
LUG 0381
LUG 0382
LUG 0383
LUG 0384
LUG 0385
LUG 0386
LUG 0387
LUG 0388
LUG 0389
LUG 0390
LUG 0391
LUG 0392
LUG 0393
LUG 0394
LUG 0395
LUG 0396
LUG 0397
LUG 0398
LUG 0399
LUG 0400
LUG 0401
LUG 0402
LUG 0403
LUG 0404
LUG 0405
LUG 0406
LUG 0407
LUG 0408

```


LUG 0409
 LUG 0410
 LUG 0411
 LUG 0412
 LUG 0413
 LUG 0414
 LUG 0415
 LUG 0416
 LUG 0417
 LUG 0418
 LUG 0419
 LUG 0420
 LUG 0421
 LUG 0422
 LUG 0423
 LUG 0424
 LUG 0425
 LUG 0426
 LUG 0427
 LUG 0428
 LUG 0429
 LUG 0430
 LUG 0431
 LUG 0432
 LUG 0433
 LUG 0434
 LUG 0435
 LUG 0436
 LUG 0437
 LUG 0438
 LUG 0439
 LUG 0440
 LUG 0441
 LUG 0442
 LUG 0443
 LUG 0444

```

    AAA2 = 0.
    AAA3 = SHEAR
    AAA4 = 0.
    IF (SHEAR) 280,282,281
  C NEGATIVE SHEAR
    280 NSEG = 2
      J1 = NT4P1
      J2 = NT8
      J3 = 1
      J4 = 1
      GO TO 285
  C POSITIVE SHEAR
    281 NSEG = 1
      J1 = 1
      J2 = NT4P1
      GO TO 285
  C APPLY TENSION
    282 IF (TENSN .EQ. 0.) GO TO 288
      J3 = 0
      J4 = 0
      IFLAG = 0
      AAA1 = 0.
      AAA2 = TENSN
      AAA3 = 0.
      AAA4 = -TENSN
      IF (TENSN) 283,288,284
  C NEGATIVE TENSION
    283 NSEG = 1
      J1 = NT2P1
      J2 = NT6P1
      GO TO 285
  C POSITIVE TENSION
    284 NSEG = 2
      J1 = NT6P1
      J2 = NT8
      J3 = 1

```

```

J4 = NT2P1
285 I = -1
JL = J1
JU = J2
DO 287 ISEG = 1, NSEG
DO 286 ILINE = J1, JU
I = I+2
IP1 = I+1
KX = IQ+NDR*(ILINE-1)
RE(KX) = RE(KX)+AAA1*SCALE(I,LOAD)+AAA2*SCALE(IP1,LOAD)
286 RE(KX+1) = RE(KX+1)+AAA3*SCALE(IP1,LCAD)+AAA4*SCALE(I,LOAD)
JL = J3
JU = J4
287 CONTINUE
IF (IFLAG.EQ. 1) GO TO 282
288 IF (IANL.EQ. 1) GO TO 289
C APPLY HALF OF LCAD AT EACH NODE AT CRACK OPENING
RE(MOVX) = 0.5*RE(LAPX)
RE(MOVY) = 0.5*RE(LAPY)
RE(LAPX) = RE(MOVX)
RE(LAPY) = RE(MOVY)
C LOADING IS COMPLETE
289 CALL BCCN(RE,IN)
C SOLUTION (POSITIVE-DEFINITE MATRIX)
ISGN = 0
CALL FACT(ISGN,RE,IN)
IF (ISGN.EQ. 1) GO TO 29
WRITE (KW,606)
GO TO 32
29 IF (IANL.EQ. 1) KT1 = 0
CALL SIMULQ(E,RE,IN)
IF (IANL.EQ. 2) GO TO 2009
C STRESS SOLUTION
REWIND 20
WRITE (KW,607) ICASE, TITLE
DO 31 L = 1, NET

```

LUG 0445
LUG 0446
LUG 0447
LUG 0448
LUG 0449
LUG 0450
LUG 0451
LUG 0452
LUG 0453
LUG 0454
LUG 0455
LUG 0456
LUG 0457
LUG 0458
LUG 0459
LUG 0460
LUG 0461
LUG 0462
LUG 0463
LUG 0464
LUG 0465
LUG 0466
LUG 0467
LUG 0468
LUG 0469
LUG 0470
LUG 0471
LUG 0472
LUG 0473
LUG 0474
LUG 0475
LUG 0476
LUG 0477
LUG 0478
LUG 0479
LUG 0480

```

CALL XTRACT(L,8,Q,RE,IN)
READ (20) E, E, V
H = E**2+V**2
DO 30 I = 1,3
  SXY(I) = 0.
DO 30 J = 1,8
  30 SXY(I) = SXY(I)+E(I,J)*Q(J)
  CSQ = E*E/H
  SSQ = V*V/H
  SC = E*V/H
  SRT(1) = SXY(1)*CSQ+SXY(2)*SSQ+2.*SXY(3)*SC
  SRT(2) = SXY(1)*SSQ+SXY(2)*CSQ-2.*SXY(3)*SC
  SRT(3) = SC*(SXY(2)-SXY(1))+(CSQ-SSQ)*SXY(3)
  IF (L.EQ. NETEF1) WRITE (KW,608)
  31 WRITE (KW,609) L, E, V, SXY, SRT
      GO TO 2011
C STRESS INTENSITY SOLUTION
2009 CALL XTRACT(NET,18,Q,RE,IN)
DO 2010 J = 1,18
  ONE(LOC) = CNE(LOC)+BCR(1,J)*Q(J)
  2010 TWO(LOC) = TWO(LOC)+BCR(2,J)*Q(J)
C CONVERT TO NASA/ASIM STANDARD STRESS INTENSITIES
  ONE(LOC) = SQPI*CNE(LOC)
  TWO(LOC) = ABS(SQPI*TWO(LOC))
C END OF LOCATION LOCP
2011 CONTINUE
IF (IANL.EQ. 1) GO TO 32
WRITE (KW,610) ICASE, TITLE
WRITE (KW,611) (LOC, ANGLE(LOC), ONE(LOC), TWO(LOC),
  2 LOC = 1, MAXLCC)
C END OF CASE
32 CONTINUE
STOP
END

```

LUG 0481
 LUG 0482
 LUG 0483
 LUG 0484
 LUG 0485
 LUG 0486
 LUG 0487
 LUG 0488
 LUG 0489
 LUG 0490
 LUG 0491
 LUG 0492
 LUG 0493
 LUG 0494
 LUG 0495
 LUG 0496
 LUG 0497
 LUG 0498
 LUG 0499
 LUG 0500
 LUG 0501
 LUG 0502
 LUG 0503
 LUG 0504
 LUG 0505
 LUG 0506
 LUG 0507
 LUG 0508
 LUG 0509
 LUG 0510
 LUG 0511
 LUG 0512
 LUG 0513
 LUG 0514